Neurobiology of Disease 212 (2025) 106966

Contents lists available at ScienceDirect

Neurobiology of Disease

journal homepage: www.elsevier.com/locate/ynbdi

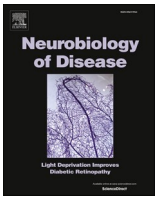

Network models incorporating chloride dynamics predict optimal strategies for terminating status epilepticus

Christopher B. Currin [a,b,*], Richard J. Burman [a,c,d,e], Tommaso Fedele [c], Georgia Ramantani [c], Richard E. Rosch [f,g], Henning Sprekeler [h], Joseph V. Raimondo [a,*]

[a] Division of Cell Biology, Department of Human Biology, Neuroscience Institute and Institute of Infectious Disease and Molecular Medicine, Faculty of Health Sciences, University of Cape Town, Cape Town, South Africa
[b] Institute of Science and Technology Austria, Klosterneuburg, Austria
[c] Department of Paediatric Neurology, University Children's Hospital Zurich and University of Zurich, Zurich, Switzerland
[d] Department of Pharmacology, University of Oxford, United Kingdom
[e] Oxford Epilepsy Research Group, Nuffield Department of Clinical Neurosciences, University of Oxford, Oxford, United Kingdom
[f] Department of Clinical Neurophysiology, King's College Hospital NHS Foundation Trust, London
[g] Wellcome Centre for Imaging Neuroscience, University College London, London, United Kingdom
[h] Bernstein Center for Computational Neuroscience Berlin, Technische Universität Berlin, Marchstr 23, Berlin, Germany

A B S T R A C T

Status epilepticus (SE), seizures lasting beyond five minutes, is a medical emergency commonly treated with benzodiazepines which enhance $GABA_A$ receptor ($GABA_AR$) conductance. Despite widespread use, benzodiazepines fail in over one-third of patients, potentially due to seizure-induced disruption of neuronal chloride (Cl^-) homeostasis. Understanding these changes at a network level is crucial for improving clinical translation. Here, we address this using a large-scale spiking neural network model incorporating Cl^- dynamics, informed by clinical EEG and experimental slice recordings. Our simulations confirm that the $GABA_AR$ reversal potential (E_{GABA}) dictates the pro- or anti-seizure effect of $GABA_AR$ conductance modulation, with high E_{GABA} rendering benzodiazepines ineffective or excitatory. We show SE-like activity and E_{GABA} depend non-linearly on Cl^- extrusion efficacy and $GABA_AR$ conductance. Critically, cell-type specific manipulations reveal that pyramidal cell, not interneuron, Cl^- extrusion predominantly determines the severity of SE activity and the response to simulated benzodiazepines. Leveraging these mechanistic insights, we develop a predictive framework mapping network states to Cl^- extrusion capacity and GABAergic load, yielding a proposed decision-making strategy to guide therapeutic interventions based on initial treatment response. This work identifies pyramidal cell Cl^- handling as a key therapeutic target and demonstrates the utility of biophysically detailed network models for optimising SE treatment protocols.

1. Introduction

Most seizures terminate within a few seconds to minutes and do so spontaneously without the need for medical intervention. There are, however, some cases where seizure activity persists and when this lasts for more than 5 mins it is termed status epilepticus (SE) (Trinka et al., 2015). SE represents a medical emergency and if seizure cessation cannot be achieved is associated with significant morbidity and even mortality (Boggs, 2004). Current first-line treatment for SE recommends the use of benzodiazepines (Glauser et al., 2016). Benzodiazepines work by increasing the conductance of chloride (Cl^-) permeable γ-amino-butyric acid (GABA) type A receptors ($GABA_ARs$), which mediate the majority of fast synaptic inhibition in the brain. The goal is to enhance inhibitory signalling to try to stop SE. Unfortunately, benzodiazepine therapy fails to halt seizures in over a third of patients, both adult and paediatric (Appleton et al., 2000; Mayer et al., 2002; Chin et al., 2008), underscoring the critical need for a deeper understanding of the mechanisms behind benzodiazepine resistance in order to develop improved treatment strategies (Burman et al., 2022).

Seizures reflect excessive excitation and synchronisation within the brain. Interneuronal populations, which release GABA and activate $GABA_ARs$ on their synaptic targets, are a principal mediator of inhibition, which typically acts to prevent the initiation or spread of seizures (Trevelyan and Schevon, 2013). The effect of fast GABAergic synaptic inhibition is dependent both on the magnitude of evoked $GABA_AR$ conductances (g_{GABA}) and the underlying reversal potential for $GABA_ARs$ (E_{GABA}) (Raimondo et al., 2017). Together these parameters control current flow through $GABA_ARs$ and consequent shifts in

* Corresponding author at: Division of Cell Biology, Department of Human Biology, Neuroscience Institute and Institute of Infectious Disease and Molecular Medicine, Faculty of Health Sciences, University of Cape Town, Cape Town, South Africa.
E-mail addresses: chris.currin+chloride@gmail.com (C.B. Currin), joseph.raimondo@uct.ac.za (J.V. Raimondo).

https://doi.org/10.1016/j.nbd.2025.106966
Received 9 December 2024; Received in revised form 22 April 2025; Accepted 18 May 2025
Available online 20 May 2025

neuronal membrane potential and firing activity (Fig. 1A). Blockade of $GABA_AR$s using pentylenetetrazole, penicillin, picrotoxin and bicuculline are classically used to induce seizures both in vitro and in vivo (Chapman et al., *1977*; Pereira de Vasconcelos et al., *1992*; Nehlig and Pereira de Vasconcelos, 1996; Pitkanen et al., *2006*; Burman et al., *2019*; El Hamdi et al., *1992*) demonstrating a strong pro-seizure effect of reducing g_{GABA}. In contrast, benzodiazepines act by enhancing the conductance of $GABA_AR$s following accompanying GABA binding (Rogers et al., 1994), and under typical conditions reduce the likelihood of seizures, demonstrating a typical anti-seizure effect of increasing g_{GABA} (Browne and Penry, 1973).

As $GABA_AR$s are primarily permeable to Cl^-, the transmembrane gradient for Cl^- sets E_{GABA} (Farrant and Kaila, 2007). It is now well accepted that the intracellular concentration of Cl^-, and hence E_{GABA}, can change over multiple timescales as a function of the cumulative Cl^- fluxes through Cl^- transporters and channels (Raimondo et al., 2012; Kaila et al., 2014). Cl^- transporters, including the cation-chloride cotransporters NKCC1 and KCC2, utilise cation gradients to import and extrude Cl^-, respectively, shifting the Cl^- gradient beyond a passive distribution (Kaila et al., 2014). Long-term changes in Cl^- cotransporter expression and function modifies steady-state E_{GABA} over development and in multiple disease states including epilepsy (Ben-Ari, 2002; Huberfeld et al., 2007). In addition to these long-term changes, short-term changes in E_{GABA} can occur when Cl^- channels such as $GABA_AR$s

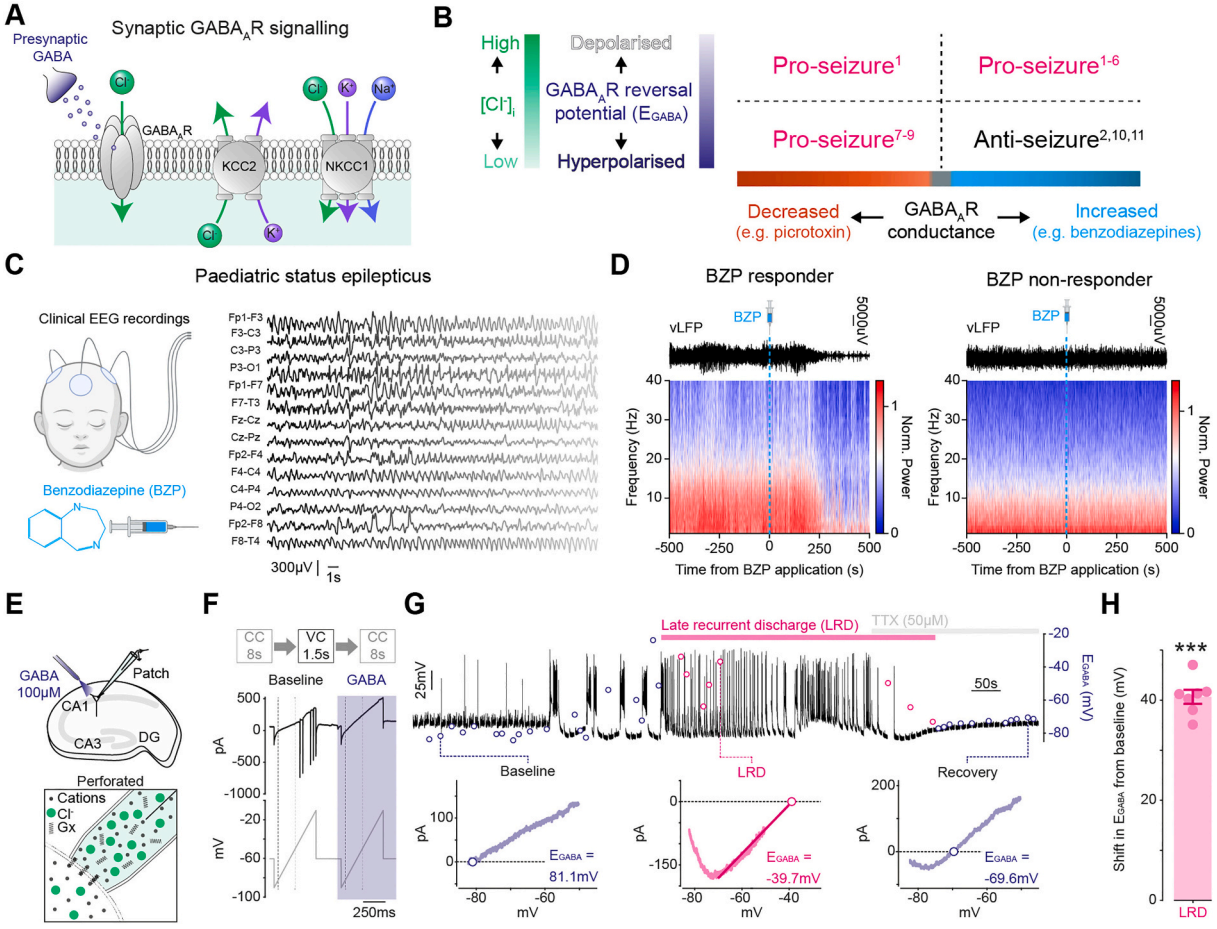

Fig. 1. The $GABA_AR$ reversal potential determines the effect of $GABA_AR$ conductance manipulation on seizures. (A) Fast GABAergic synaptic inhibition is mediated by $GABA_AR$s, which are predominantly permeable to Cl^-. Upon GABA binding, Cl^- flows down its electrochemical gradient depending on the reversal potential for $GABA_AR$s (E_{GABA}) and the membrane potential. E_{GABA} is predominantly a function of the Cl^- gradient, which is modulated by the action of the Cl^- transporters KCC2 and NKCC1. (B) A table with references to experimental papers demonstrating a variable effect of $GABA_AR$ modulation on seizures depending on E_{GABA} (Burman et al., 2019; Sivakumaran and Maguire, 2016; Staley, 1992; Deeb et al., 2012; Deshpande et al., 2007; Codadu et al., 2019; Chapman et al., 1977; Nehlig and Pereira de Vasconcelos, 1996; El Hamdi et al., 1992; Cheung et al., 2022; Jarvis et al., 2023). Increasing $GABA_AR$ conductance with benzodiazepines can either be pro-seizure or anti-seizure depending on E_{GABA}. (C) Clinical EEG recordings from a paediatric patient in status epilepticus (data from (Fedele et al., 2025)). (D) Virtual local field potential recordings (vLFP) extracted from 21-channel EEG recordings with corresponding power spectra. Epochs consist of 500 s on either side of benzodiazepine administration. One example shows a clear reduction in electrical activity following benzodiazepine administration ('BZP responder') whilst the other shows an example of a patient in which the benzodiazepine did not modify the EEG signal ('BZP non-responder'). (E) Schematic depicting experimental setup of gramicidin perforated patch-clamp recordings from pyramidal cells in organotypic hippocampal brain slice cultures and accompanying somatic GABA application. (F) To measure E_{GABA} during seizure-like activity, the recording mode was rapidly switched from current-clamp (CC, 8 s duration) to brief periods in voltage clamp (VC, 1.5 s duration) every 10 s *(data from 14)*. While in VC, two consecutive voltage ramps (bottom trace) were applied: the first without GABA application and the second with GABA application (purple) directed toward the soma. The current was recorded (top trace) and a subtraction performed to calculate the GABA current and E_{GABA}. (G) A representative recording from a CA1 pyramidal neuron where E_{GABA}. measurements (dots) were made during the evolution of epileptiform activity in the 0 Mg^{2+} model (pink bar denotes the Late Recurrent Discharge phase, LRD, akin to Status Epilepticus). Dotted lines highlight different periods during the progression of epileptiform activity: baseline, during LRD, and following termination of activity / post-LRD with TTX (50 mM). Bottom, I-V plots were used to calculate E_{GABA} defined as the voltage at which the GABA current equals 0. (H) Population data demonstrating a profound shift in E_{GABA} from baseline (mean shift: 40.67 ± SEM 1.38 mV, $N = 7$, $^{***}P < 0.001$, one-sample *t*-test). (For interpretation of the references to colour in this figure legend, the reader is referred to the web version of this article.)

are intensely activated causing Cl^- influx that overwhelms Cl^- extrusion mechanisms (Raimondo et al., 2012). In vitro and in vivo data from animal models has shown that this occurs during seizures and SE where intracellular Cl^- accumulation and a depolarising shift in E_{GABA} can reduce the inhibitory effectiveness of GABAergic interneuronal cell populations, or even render them excitatory (Ellender et al., 2014; Sulis Sato et al., 2017; Magloire et al., 2019).

The modulation of g_{GABA} is commonly used to control seizure activity both in the clinic and the laboratory. Various data from patients and animal models have demonstrated that the effect of g_{GABA} modulation on seizures depends on the underlying transmembrane Cl^- gradient and E_{GABA}. A reduction in g_{GABA}, including via blockade of $GABA_AR$ using picrotoxin or bicuculline, is typically pro-seizure causing hyperexcitability regardless of E_{GABA} (Burman et al., 2019; Miles et al., 1984; Viitanen et al., 2010; Wenzel et al., 2017) (Fig. 1B). In contrast, enhancing g_{GABA} with positive allosteric modulators of $GABA_ARs$, such as benzodiazepines, can have an anti-seizure effect when intracellular Cl^- concentration and E_{GABA} are low (Sivakumaran and Maguire, 2016; Cheung et al., 2022; Jarvis et al., 2023) but can have no effect, or a pro-seizure effect when intracellular Cl^- concentration and E_{GABA} are high (Burman et al., 2019; Sivakumaran and Maguire, 2016) (Fig. 1B). SE and how it is affected by pharmacological perturbation is the result of multiple dynamically interacting mechanisms between different cell-types in brain networks, which can be difficult to predict or to study experimentally. Computational models allow for simulations of the effects of individual parameter on neuronal dynamics and therefore are an ideal tool to complement experiments for ascertaining the mechanistic underpinnings of the clinically relevant phenomenon of benzodiazepine resistant SE, and for designing improved therapeutic strategies. Previous computational models incorporating Cl^- dynamics have been successfully used to demonstrate the importance of Cl^- in affecting synaptic integration and information processing by single cells (Doyon et al., 2011; Jedlicka et al., 2011a; Currin et al., 2020; Currin et al., 2022).

Here we present a large spiking neural network model incorporating Cl^- dynamics, informed by data from human electroencephalography (EEG) recordings of SE and experimental brain slice recordings, to better understand and address the phenomenon of benzodiazepine resistance in SE. By employing a large-scale network, this approach allows us to investigate emergent, network-level dynamics and cell-type specific contributions related to chloride homeostasis, extending beyond previous single-cell or mean-field models. Our simulations show that the $GABA_AR$ reversal potential establishes SE-like bursting and dictates the network's response to $GABA_AR$ conductance modulation, aligning with experimental observations. We further reveal that steady-state bursting activity and E_{GABA} depend on a non-linear interaction between $GABA_AR$ conductance and the strength of Cl^- extrusion, but not the initial E_{GABA}. Critically, by separately manipulating Cl^- extrusion in different neuronal populations, we uncover the dominant role of pyramidal cell Cl^- extrusion in determining SE-like activity severity and the response to simulated benzodiazepine application. Leveraging these mechanistic insights, we demonstrate the model's utility for conceptualising improved therapeutic protocols, proposing a novel, mechanistically-grounded framework based on the cell-type specific role of Cl^- extrusion for more rapidly terminating SE in the clinic.

2. Results

2.1. The $GABA_AR$ reversal potential determines the effect of $GABA_AR$ conductance manipulation on seizures

To illustrate the clinical presentation of benzodiazepine-resistant SE, we extracted example EEG recordings from paediatric patients (data from (Fedele et al., 2025)). A unique feature of these recordings is that they capture the pre- and post-effect of benzodiazepine application during SE. Notably in one patient, enhancing g_{GABA} with a benzodiazepine resulted in the cessation of the EEG readout of seizure activity over the course of minutes ('BZP responder', Fig. 1C and D). However, in another patient, benzodiazepine application had no effect on seizure activity ('BZP non-responder', Fig. 1D). While it is not currently feasible to measure intracellular Cl^- concentration or E_{GABA} in human patients, one can use animal models to study SE and use them as a proxy to gain mechanistic insights into how $GABA_AR$ physiology changes during persistent seizure activity. Here, we demonstrate from previous experimental data (Burman et al., 2019) that withdrawing Mg^{2+} from the perfusing solution of organotypic brain slice cultures can reproduce SE-like activity. Using this in vitro model, gramicidin perforated patch-clamp recordings are used to measure the E_{GABA} throughout the evolution of SE-like activity without perturbing intracellular Cl^- (Fig. 1E and F). Through this data, we can observe how the E_{GABA} undergoes a significant depolarising shift from baseline (mean shift: 40.67 ± SEM 1.38 mV, $N = 7$, $^{***}P < 0.001$, one-sample t-test) when it enters a period of late recurrent discharges (LRD) that is electrographically similar to SE (Fig. 1G and H). Stopping SE-like activity using tetrodotoxin returned E_{GABA} to more negative values. This seizure-associated shift in E_{GABA} explains why if a benzodiazepine is applied before or at the onset of a seizure in this model, the seizure-like activity can be prevented, delayed, or reduced (Burman et al., 2019). However, if benzodiazepines are applied during status epilepticus-like activity, when E_{GABA} is elevated, network activity may remain unaffected or exacerbated (Burman et al., 2019).

2.2. A network model of status epilepticus is suppressed or enhanced by increased $GABA_AR$ conductance depending on the neuronal $GABA_AR$ reversal

To investigate the effect of E_{GABA} on how modulation of g_{GABA} affects seizure activity, we built a spiking neural network model consisting of leaky integrate-and-fire point neurons: 800 pyramidal cells (PC) and 200 interneurons (IN). These were interconnected and received a low level of constant, external excitatory drive (Fig. 2A and Methods). E_{GABA} was set at the same constant, static value in all cell types. Incrementing E_{GABA} by 4 mV every 40 s of simulation from −74 mV until −38 mV showed that E_{GABA} strongly controls firing rate bursts in the network, with no bursting being observed with E_{GABA} less than −60 mV (Fig. 2B and C). E_{GABA} values above −60 mV resulted in bursting comparable to the network bursts observed in experimental models of SE (Burman et al., 2019) and Fig. 1G.

Analysis of the model mechanisms indicated that large NMDA conductances primarily drove the peak firing during bursts (Fig. S1C), while the depletion of finite glutamate vesicle pools was crucial for burst termination (Fig. S1D, and see Supplementary Information S3 for details and Fig. S3). Although NMDA activity (not blocked by Mg^{2+}) shapes the bursts, a sufficiently depolarised E_{GABA} is permissive for their generation in this model (Fig. 2B, Fig. S1B). Furthermore, although Fig. 2 illustrates findings for our default parameters, the qualitative effects of E_{GABA} and $g_{GABAmax}$ on bursting were robust to variations in network size (Fig. S2A) and alternative external input configurations (Fig. S2B, see Supplementary Information S4 for more details).

Next, we sought to simulate the experiments described in Fig. 1 by using our spiking neural network model to computationally determine how different neuronal E_{GABA} values might modify the effect of g_{GABA} modulation on seizure-like activity (bursts of increased population firing rate). To do so, after running the network simulation for 300 s with a "normal" g_{GABA} ($g_{GABAmax}$) of 50 nS, $g_{GABAmax}$ was altered to be either 4× smaller (e.g. modelling "picrotoxin" application, a $GABA_AR$ antagonist) or 4× larger (e.g. modelling "benzodiazepine" application, a positive $GABA_AR$ conductance modulator) (Fig. 2D-H). To model the effects of different underlying E_{GABA} on this manipulation, the simulations were repeated using E_{GABA} of −74 mV (hyperpolarising), −60 mV (shunting) or − 46 mV (depolarising). For hyperpolarising E_{GABA} (−74 mV, Fig. 2D, left column), the network transitioned to occasional bursting following simulated picrotoxin application (12.5 nS $g_{GABAmax}$)

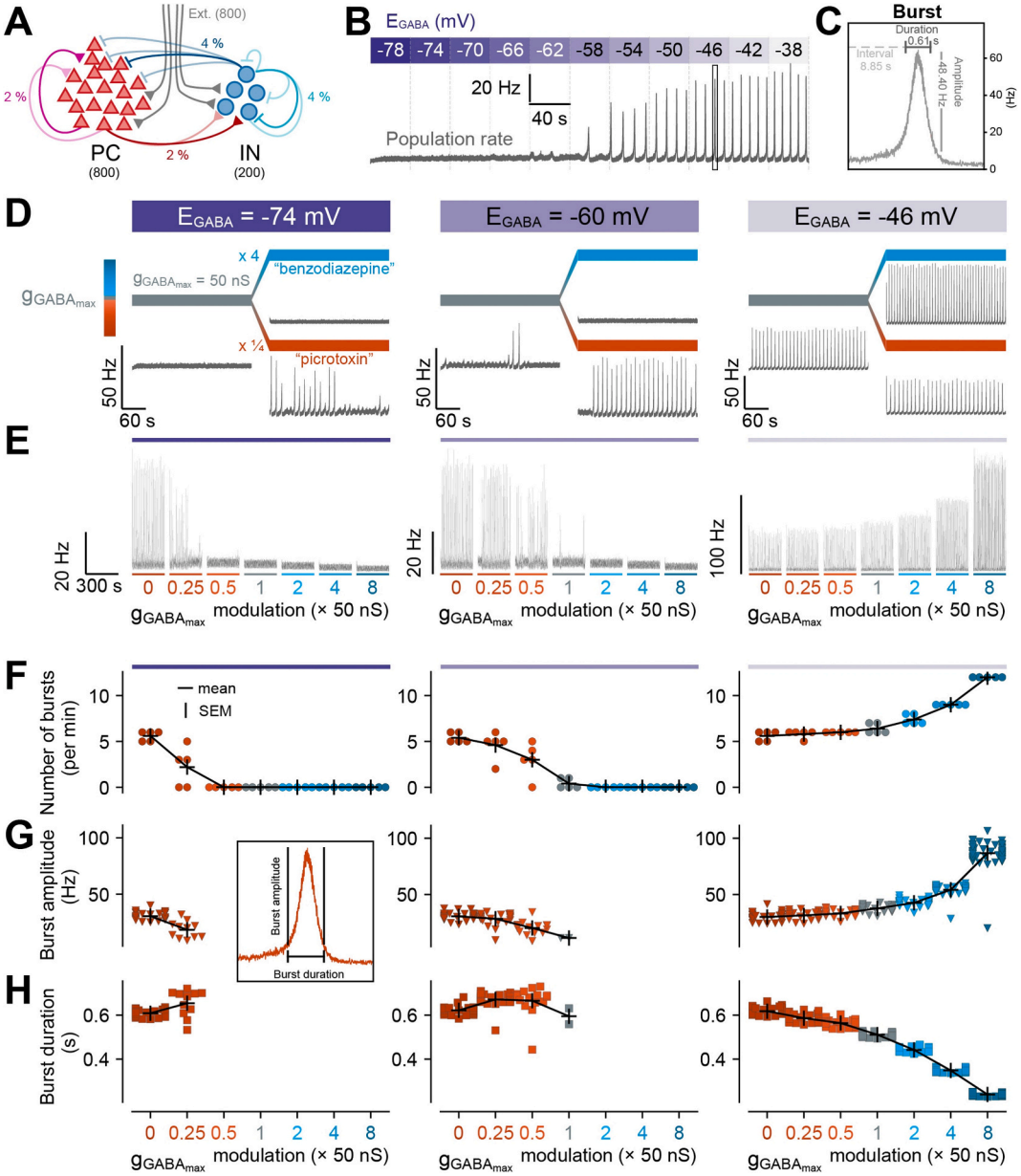

Fig. 2. $GABA_AR$ reversal sets epileptiform bursting in a network model and determines the response to $GABA_AR$ conductance modulation. (A) Schematic of the spiking neural network model consisting of 800 pyramidal cells (PC) and 200 interneurons (IN), with 800 low frequency (2 Hz) and low weight (2 nS $g_{AMPAmax,2Hz}$) external inputs. The connection probabilities (in %) between and within populations are as follows: PC → PC: 2 %, PC → IN: 2 %, IN → IN: 4 %, IN → PC: 4 %. (B) E_{GABA} (purple scale bar) was altered at discrete time points, every 40 s, by 4 mV, from −78 mV until −38 mV. The population firing rate was monitored for bursts (C), detected as twice the standard deviation of the mean, above 20 Hz and for at least 20 ms. (D) Average firing rate of neurons with hyperpolarising E_{GABA} (left: −74 mV), shunting E_{GABA} (middle: −60 mV) or depolarising E_{GABA} (right: −46 mV). After 300 s of normal $GABA_AR$ conductance ($g_{GABAmax}$ = 50 nS, grey bar), $g_{GABAmax}$ was either negatively (× ¼, simulating picrotoxin, orange bar) or positively modulated (× 4, simulating benzodiazepine, blue bar). Note simulated benzodiazepine application silencing bursting at a shunting E_{GABA} (middle), but exacerbating bursting when E_{GABA} is depolarised (right). (E) Population firing rates for a range of $g_{GABAmax}$ modulations (as a proportion of 50 nS). (F) The number of bursts for each $g_{GABAmax}$ modulation. Each coloured marker indicates the number of bursts per minute. Black crosses indicate the mean values. (G) The amplitude of bursts for each $g_{GABAmax}$ modulation. Each coloured marker indicates a burst. (H) The duration of bursts for each $g_{GABAmax}$ modulation. Each coloured marker indicates a burst. For each simulation, E_{GABA} was kept constant over the entire 600 s duration, and $g_{GABAmax}$ was modulated at 300 s. The population rate statistics were calculated over 300 s of the respective simulation of that condition ($N = 5$). (For interpretation of the references to colour in this figure legend, the reader is referred to the web version of this article.)

or remained quiescent following simulated benzodiazepine application (200 nS $g_{GABAmax}$). At a shunting E_{GABA} (−60 mV, Fig. 2D, middle column), the network transitioned from sporadic bursts to either continuous bursting following "picrotoxin" or was silenced following "benzodiazepine" application. Finally, at depolarising E_{GABA} (−46 mV, Fig. 2D, right column), the network exhibited continuous bursting at baseline. The simulated application of picrotoxin by reducing $g_{GABAmax}$ did not substantially change the network behaviour. However, positively modulating $g_{GABAmax}$ (simulating application of a benzodiazepine) not only did not reduce bursting, but instead substantially increased it.

In addition to "benzodiazepine", we simulated the effects of "low dose phenobarbital", which positively modulates $g_{GABAmax}$ (Fig. S4B), and "high dose phenobarbital", which modulates $g_{GABAmax}$ as before but also negatively modulates maximum AMPA conductances ($g_{AMPAmax}$, Fig. S4C). The additional effect of reducing $g_{AMPAmax}$ caused the network

to be silenced, even at depolarised E_{GABA}, with the mean population activity below baseline levels of conductances and E_{GABA} (Fig. S4D). See Supplementary Information S5 for details.

To examine the graded effect of $g_{GABAmax}$ modulation, the procedure was repeated for a range of $g_{GABAmax}$ values from 12.5 nS to 400 nS (and 0 nS, Fig. 2E). The number of bursts per min (Fig. 2F), the amplitude of bursts (maximum firing rate minus firing rate at start of burst, Fig. 2G) and the duration of bursts (period of time when the firing rate was above 20 Hz, Fig. 2H) were calculated. Together these simulation results corroborate the experimental results by demonstrating that at hyperpolarised E_{GABA}s and shunting E_{GABA}s, reducing g_{GABA} in the network elicits SE-like activity in the form of repeated bursting with increased g_{GABA} silencing the bursting activity. In contrast at a depolarised E_{GABA}, increasing g_{GABA} increased the amplitude and frequency of bursting representing an exacerbation of SE-like activity. As part of the network sensitivity analysis (Supplementary Information S4), we also assessed how the number of bursts depends on $g_{AMPAmax}$ and $g_{NMDAmax}$ (Fig. S3), with NMDA strongly contributing to an increased number of bursts.

2.3. Chloride extrusion controls network bursting and the response to GABA conductance modulation

In the previous simulations intracellular Cl^- concentration, E_{Cl} and hence E_{GABA} were treated as static parameters. However, it is more accurate to consider these parameters as dynamic variables because intracellular Cl^- fluctuates as a function of activity-dependent Cl^- flux

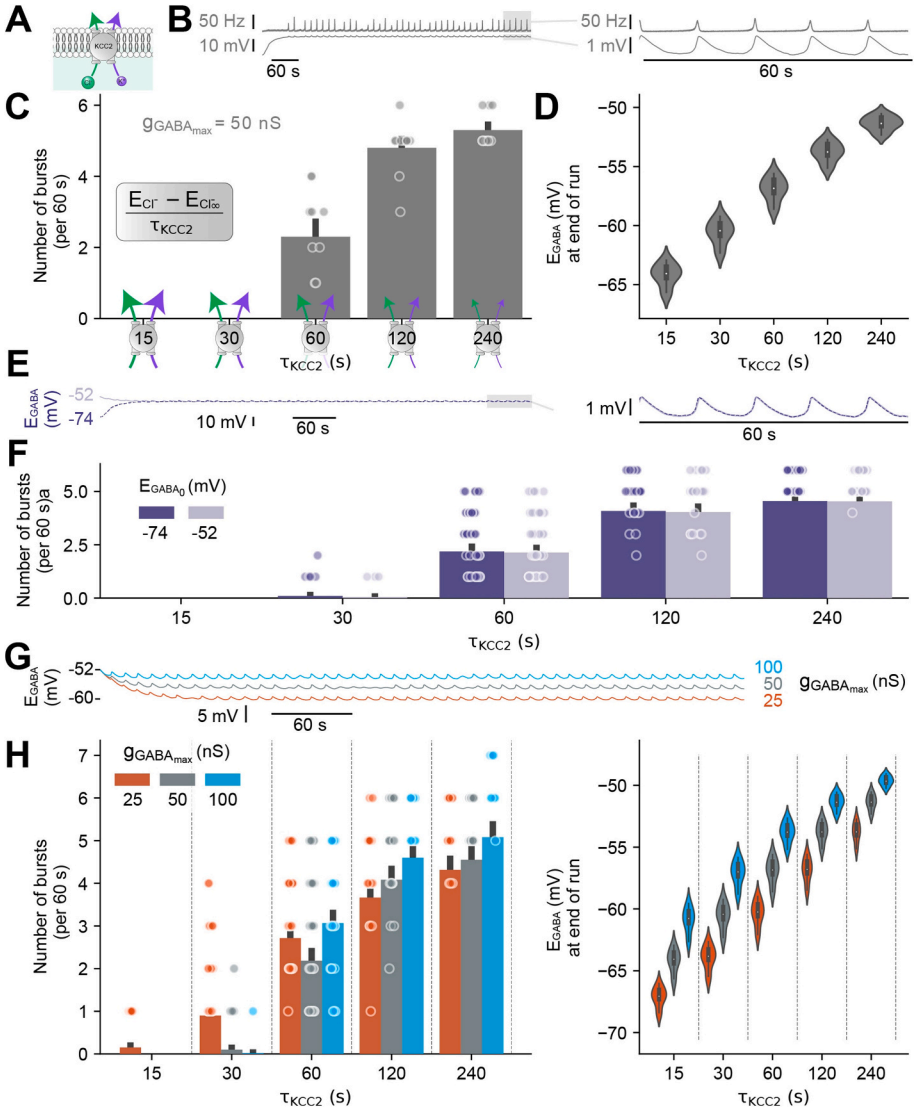

Fig. 3. Chloride extrusion controls network bursting and the response to $GABA_AR$ conductance modulation. (A) Schematic of the primary Cl^- extrusion mechanism in adult neurons (KCC2) which is modelled as a single exponential decay to baseline (−88 mV) that depends on the time constant (τ_{KCC2}). Smaller values of τ_{KCC2} indicate faster extrusion rates. (B) A simulation with dynamic Cl^- whereby E_{GABA} (bottom trace) depends on τ_{KCC2} (60 s) and the population activity (top trace) responds to elevated E_{GABA} by bursting. E_{GABA} initialised at −74 mV. Inset, zoom of traces showing ~1 mV change in E_{GABA} in response to bursts. (C) The number of network bursts (per min) depended on the Cl^- extrusion strength (τ_{KCC2}), with slower extrusion causing more bursts. (D) Reduced Cl^- extrusion (slower τ_{KCC2}) resulted in elevated steady-state E_{GABA}. (E) E_{GABA} did not depend on the initial E_{GABA} (E_{GABA0}). For simulations with E_{GABA0} of either −74 mV (dark purple, dashed) or − 51.6 mV (light purple, solid), the resulting steady-state E_{GABA} was the same. Inset, the traces for −74 mV and − 51.6 mV E_{GABA0} are overlapping. Note that the same seed was used in both traces. (F) The number of bursts per min were independent of E_{GABA0}. Black bars show the standard error of the mean (SEM). (G) E_{GABA} traces for different values of $g_{GABAmax}$ (25 nS: orange, 50 nS: grey, 100 nS: light blue). All simulations started at −51.6 mV. (H) Histogram of the number of bursts per min and (I) violin plots of steady-state E_{GABA} for different values of $g_{GABAmax}$ and τ_{KCC2}. Each coloured marker indicates the number of bursts over the last 5 min of a 10-min simulation ($N = 10$ simulations per condition). Violin plots include a box-and-whisker plot inside with the median value indicated as a white marker. (For interpretation of the references to colour in this figure legend, the reader is referred to the web version of this article.)

through $GABA_AR$s and Cl^- extrusion via the cation-chloride cotransporters such as KCC2 (Fig. 3A). Therefore, in this set of simulations the evolution of E_{GABA} over time was modelled as a dynamic variable (see Materials and Methods). The efficacy of Cl^- extrusion in each neuron could be set by changing τ_{KCC2}, the time constant of E_{Cl} (and hence E_{GABA}) recovery, with slower τ_{KCC2} of 60 s or more representing reduced Cl^- extrusion by KCC2. We found that τ_{KCC2} determined the number of bursts in the network (Fig. 3B and C) as well as the ultimate steady-state E_{GABA} (Fig. 3B and D). Slower τ_{KCC2} values with resultant reduced Cl^- extrusion led to the network generating multiple bursts per minute together with elevated average steady-state E_{GABA}. Whilst E_{GABA} was dynamic during simulations, changing from its initial value as well as rising and falling in response to individual network bursts (Fig. 3B, inset), we found that the initial E_{GABA} (E_{GABA0}) did not affect the final steady state E_{GABA} (Fig. 3E and F), which was instead affected by the strength of Cl^- extrusion (τ_{KCC2}).

As Cl^- influx via activated $GABA_AR$s also affects E_{GABA} (see Fig. 3B inset) we next sought to determine how modulation of $g_{GABAmax}$ (akin to blockade or enhancement of $GABA_AR$s using picrotoxin or benzodiazepines respectively), might affect seizure-like activity in the context of dynamic Cl^- and E_{GABA}. We first monitored E_{GABA} in networks with the same level of neuronal Cl^- extrusion (τ_{KCC2}) but with different $g_{GABAmax}$values of 25 nS, 50 nS, and 100 nS. Steady state neuronal E_{GABA} was substantially different between the conditions, with a difference of 9 mV between the low and high $g_{GABAmax}$ conditions (Fig. 3G). Next, to determine the interaction between Cl^- extrusion, $GABA_AR$ conductance and seizure-like activity, we systematically altered $GABA_AR$ conductance ($g_{GABAmax}$) at different Cl^- extrusion rates (τ_{KCC2}) and counted the number of network bursts (Fig. 3H, Fig. S5) together with measuring steady state E_{GABA} (Fig. 3I). In networks with enhanced Cl^- extrusion (short τ_{KCC2}) and resultant hyperpolarised steady state E_{GABA}s, reduced $GABA_AR$ conductance (orange) increased bursting while enhanced $GABA_AR$ conductance (blue) silenced the networks. In contrast, in networks with low extrusion rates (long τ_{KCC2}) and depolarised steady state E_{GABA}s, reducing $GABA_AR$ conductance reduced bursting whilst increasing $GABA_AR$ conductance (akin to benzodiazepine application) exacerbated bursting.

2.4. Compromised chloride extrusion in the pyramidal cell population is the major determinant of network bursting

Thus far, to determine the effects of compromised Cl^- extrusion on SE-like activity as represented by network bursting, we have manipulated Cl^- extrusion (by adjusting τ_{KCC2}) in all neurons. To investigate how Cl^- extrusion in specific neuronal subpopulations might affect SE-like activity, we altered Cl^- extrusion either in the pyramidal cell (PC) or interneuronal (IN) populations alone. With a view to understanding potential cell-type specific modulation of Cl- extrusion to affect SE, in these simulations E_{GABA} was initially set at a depolarised, SE-like level of −51.6 mV and allowed to evolve dynamically thereafter. Using a "baseline" $g_{GABAmax}$ of 50 ns, it was immediately apparent that Cl^- extrusion in pyramidal cells (τ_{KCC2PC}) strongly determined bursting activity (Fig. 4A, B and D). Strong Cl^- extrusion in pyramidal cells ($\tau_{KCC2PC} < 15$ s) terminated network bursts whilst progressively weaker Cl^- extrusion resulted in increased bursting (Fig. 4B, D). In comparison, modulation of Cl^- extrusion exclusively in the GABAergic interneuronal population (τ_{KCC2IN}) had a substantially smaller effect on bursting activity (Fig. 4C and D).

The strength of $GABA_AR$ conductance modulated the effect of cell type specific Cl^- extrusion on network bursting (Fig. E and F). Increasing $g_{GABAmax}$ (Fig. E) decreased the number of bursts at strong (i.e. short) τ_{KCC2PC} but increased the number of bursts substantially at weak (i.e. slow) τ_{KCC2PC}. This was in line with the previous results. Although modulation of τ_{KCC2IN} had much smaller effects on network bursting, trends could be observed particularly following manipulation of $g_{GABAmax}$. At a baseline $g_{GABAmax}$ of 50 nS (grey), the total number of bursts

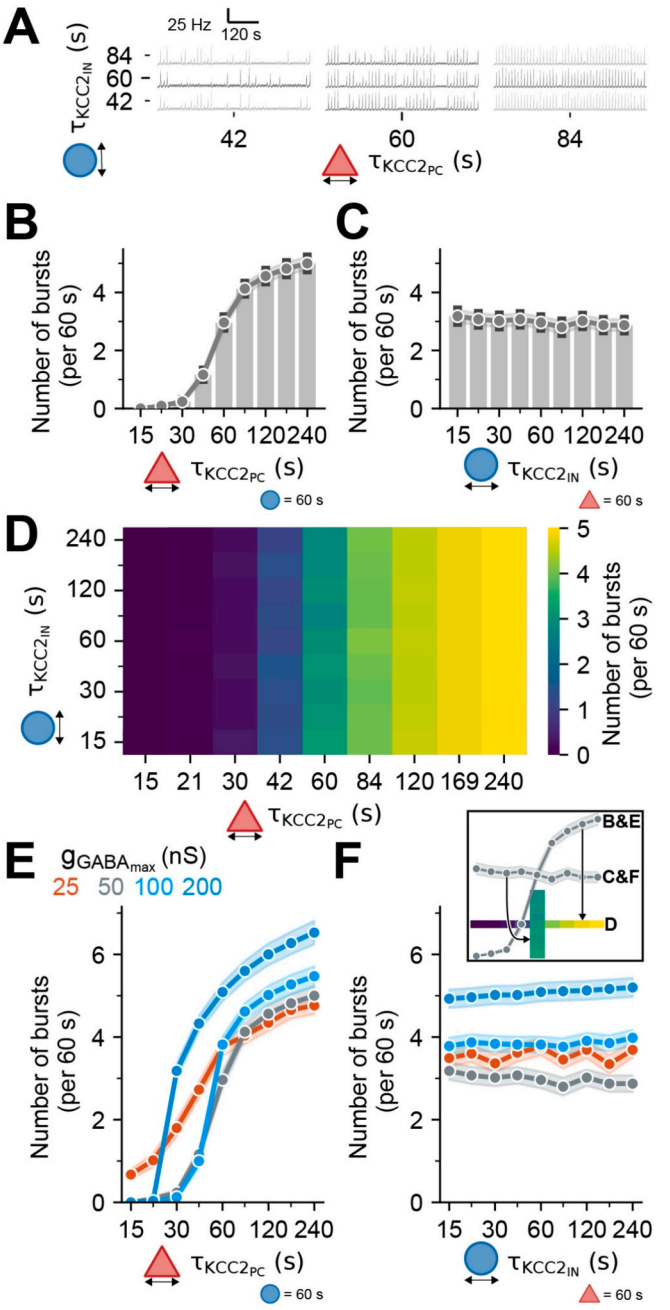

Fig. 4. Compromised chloride extrusion in the pyramidal cell population is the major determinant of network bursting. (A) Population firing rate traces where τ_{KCC2} was independently varied for the pyramidal cell (τ_{KCC2PC}) and interneuron (τ_{KCC2IN}) populations respectively. For all simulations, E_{GABA} was initialised at −51.6 mV. (B) Histograms of the number of bursts versus τ_{KCC2PC} ($\tau_{KCC2IN} = 60$ s) or (C) τ_{KCC2IN} ($\tau_{KCC2PC} = 60$ s). Black bars indicate ± SEM, $N = 5$ simulations. (D) Heatmap of the average number of bursts for a matrix of τ_{KCC2IN} and τ_{KCC2PC} values. The average is calculated from 5 separate simulations. (E) Line plots of the number of bursts versus τ_{KCC2PC} ($\tau_{KCC2IN} = 60$ s) or (F) τ_{KCC2IN} ($\tau_{KCC2PC} = 60$ s), for values of $g_{GABAmax}$ (25 nS: orange, 50 nS: grey, 100 nS: light blue, 200 nS: darker blue). Shaded areas indicate SEM, N = 5 simulations. The inset shows the relation between the heatmap and the bar and line plots. (For interpretation of the references to colour in this figure legend, the reader is referred to the web version of this article.)

decreased with slower τ_{KCC2IN}. In contrast at a high $g_{GABAmax}$ the number of bursts increased with slower τ_{KCC2IN} (Fig. F). Overall, these results highlight the importance of the PC population's Cl^- extrusion capacity, over that of the IN population, for managing network activity and

preventing SE-like activity.

2.5. Interacting chloride plasticity mechanisms determine the optimal approach for terminating network bursts

So far, we separately compared how SE-like activity in the form of network bursting is affected by $GABA_AR$ reversal potential (E_{GABA}), $GABA_AR$ conductance ($g_{GABAmax}$) and neuronal Cl^- extrusion (τ_{KCC2}). Here, we investigated how all three of these variables interact in a way that could help guide future strategies for medical intervention in SE (Fig. 5). First, we used a network with static Cl^- where E_{GABA} was held constant at different values. Positively modulating $g_{GABAmax}$ from a baseline of 0 nS $g_{GABAmax}$ decreased the number of bursts when $E_{GABA} < -52$ mV but increased the number of bursts when $E_{GABA} > -52$ mV (Fig. 5A). This showed that $g_{GABAmax}$ modulation had different trajectories for different E_{GABA}s. If initial $g_{GABAmax}$ modulation did not reduce the rate of bursting, further $g_{GABAmax}$ modulation only served to exacerbate network activity further. This suggests that in the clinic, having EEG feedback to determine the response to initial benzodiazepine treatment could be useful for determining next treatment steps, particularly where seizure activity is not aborted.

To extend this idea further, we included the more realistic scenario of dynamic Cl^- and how neuronal Cl^- extrusion complicates the relationship between $GABA_AR$ conductance and synchronised bursting activity in the network. This is important because τ_{KCC2} and $g_{GABAmax}$ together control to what extent bursting activity raises E_{GABA} in a positive feedback loop (see Fig. 3H and the equation for $\frac{d}{dt}E_{Cl^-}$ in Materials and Methods). By plotting the number of network bursts as a function of $g_{GABAmax}$ and τ_{KCC2} together with E_{GABA}, useful observations were made. Firstly, different combinations of τ_{KCC2} and $g_{GABAmax}$ determine whether a network bursts and whether increasing $g_{GABAmax}$ will decrease or increase bursting (Fig. 5B). Given a network which is bursting (or a patient in SE), with no other information, it is not possible to know what the likely effect of increasing $GABA_AR$ conductance (i.e. benzodiazepine treatment) will be. However, by measuring the response (extent of network bursting) to increasing $g_{GABAmax}$ ("benzodiazepine treatment", blue arrows), one can then determine where in the network "landscape" one is positioned to choose the optimum next step to increase the likelihood of terminating seizures. We summarise this as a decision tree in Fig. 5C. If raising $g_{GABAmax}$ (blue arrow) reduces bursting, then the network is in Regime 1 (magenta). $g_{GABAmax}$ can then be raised further. If raising $g_{GABAmax}$ increases bursting, then the network is in Regime 2 (orange). In this case, $g_{GABAmax}$ should be reduced by halting further benzodiazepine treatment. In addition, neuronal Cl^- extrusion should be increased if possible (green arrow). We note that pharmacological enhancers of Cl^- extrusion are not yet clinically available. Nonetheless, our modelling results demonstrate how in the case that $GABA_AR$ conductance increases network activity in SE, an optimal strategy for suppressing persistent seizures would be to reduce $GABA_AR$ conductance together with enhancing Cl^- extrusion.

3. Discussion

In this study, we used computational models informed by clinical and experimental data to investigate the phenomenon of benzodiazepine resistance in status epilepticus. Here we leverage the unique capabilities of a large-scale spiking neural network incorporating Cl^- dynamics – a novel approach for studying SE – to demonstrate the effects of dynamically shifting Cl^- gradients on network behaviour, a necessary step given recent experimental demonstrations of profound Cl^- fluctuations during seizures (Burman et al., 2019; Magloire et al., 2019). Our model confirms and extends experimental evidence, showing that the neuronal $GABA_AR$ reversal potential (E_{GABA}) determines the impact of $GABA_AR$ conductance ($g_{GABAmax}$) modulation on SE-like activity. Key novel contributions derived from this approach include the elucidation of the dominant role of pyramidal cell Cl^- extrusion in controlling network bursting, and the development of a predictive framework with direct translational potential for guiding SE treatment. Furthermore, our results indicate that considered modulation of both $GABA_AR$ conductance and Cl^- extrusion is optimal for arresting SE-like activity.

We constructed our computational spiking neural network model to align with the well-characterised in vitro 0 Mg^{2+} brain slice model of acute, convulsive SE. As during in vitro experiments, transitioning the

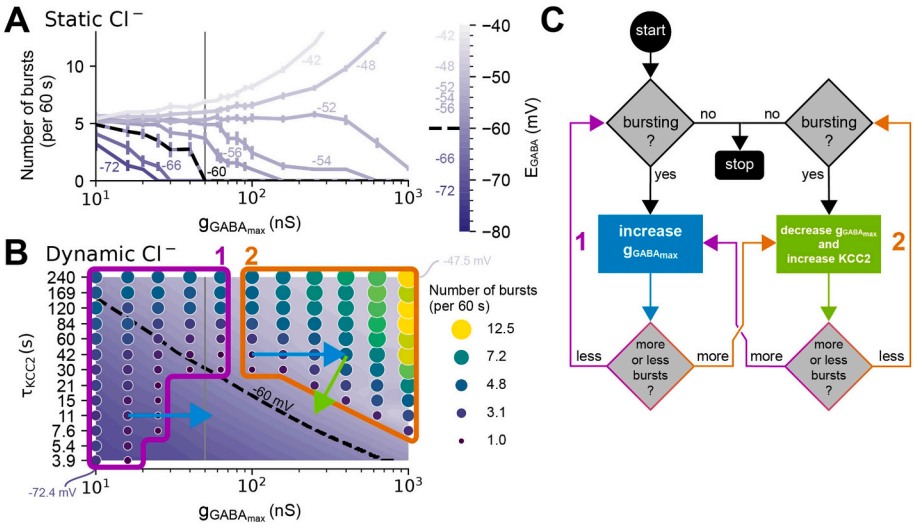

Fig. 5. Interacting chloride plasticity mechanisms determine the optimal approach for terminating network bursts. (A) For simulations with static Cl^-, the effect of positively modulating GABA conductance ($g_{GABAmax}$) on a network's bursting frequency depends on E_{GABA} (purple lines ± SEM, $N = 10$ simulations per condition, 60 s each). E_{GABA} was varied from −74 mV to −42 mV in increments of 2 mV. (B) Burst frequency as a function of $g_{GABAmax}$ and τ_{KCC2} in simulations with dynamic Cl-, plotted together with average E_{GABA}. E_{GABA} was measured at either the time of a burst or after 600 s if there were no bursts. Dashed line represents $E_{GABA} = -60$ mV, with the colourmap displayed in discrete 1 mV intervals. Low $g_{GABAmax}$ elicits bursting behaviour regardless of τ_{KCC2}. Increasing $g_{GABAmax}$ decreases bursts if τ_{KCC2} is fast enough. Application of positive $g_{GABAmax}$ modulation (blue arrows, simulating benzodiazepine application) decreases bursting at fast (short) τ_{KCC2} indicating that the network is in Regime 1 (magenta) but increases bursting at slow (long) τ_{KCC2}, indicating that the network is in Regime 2 (orange). Recovery from bursting in Regime 2 can be facilitated by reducing $g_{GABAmax}$ and increasing Cl^- extrusion (green arrow). (C) Decision tree depicting the optimal strategy for terminating seizures in SE based on the simulations in 'B'. (For interpretation of the references to colour in this figure legend, the reader is referred to the web version of this article.)

network to recurrent firing-rate bursts representing SE-like activity is linked with an elevation of E_{GABA} (i.e. raised $[Cl^-]_i$). Network bursting is affected by multiple factors including the properties of neurotransmitter release, receptor conductances, network size and connectivity (Melamed et al., 2008; Gerstner et al., 2014) (see also Figure S3). Nonetheless, we could confirm that E_{GABA} was always a principal factor in transitioning a network from stable to bursting, SE-like behaviour.

The application of in silico pharmacological treatment to modulate $g_{GABAmax}$ corroborated experimental results and highlighted the contrasting behaviour of increasing $g_{GABAmax}$, which is anti-seizure at low, physiological E_{GABA}, but pro-seizure at high, pathological E_{GABA} (Burman et al., 2020; Wang et al., 2018). In our model, the "edge" for transitioning between these two respective effects was an E_{GABA} of −60 mV. Experimental data suggest that the longer seizure activity continues unabated, the more likely it is that neurons undergo intracellular Cl^- accumulation and a positive shift in E_{GABA} (Burman et al., 2019; Rivera et al., 2004; Lee et al., 2011). This, together with our modelling data, helps provide a mechanistic explanation for the clinical observation that patients with SE who seize for longer prior to initial treatment are more likely to be resistant to benzodiazepine treatment (Burman et al., 2022; Burman et al., 2019; Gaínza-Lein et al., 2018).

Previous work has shown that the continued seizure activity that occurs during SE results in internalisation of $GABA_A$Rs (Kapur and Coulter, 1995; Goodkin et al., 2005), which both progressively exacerbates seizures and impairs the potential effectiveness of benzodiazepines as anti-seizure agents. This is because the ability of benzodiazepines to increase $g_{GABAmax}$ is compromised by a lack of $GABA_A$Rs with the requisite subunits (Goodkin et al., 2008). Until recently this has been suggested as the major mechanism underlying benzodiazepine resistance in SE. Our model shows the importance of both changes in $g_{GABAmax}$ together with activity-dependent dynamics in Cl^- and E_{GABA} for predicting the effectiveness of benzodiazepine resistance in SE.

A powerful determinant of how readily neuronal E_{GABA} increases following activity-dependent Cl^- influx through $GABA_A$Rs is the strength of neuronal Cl^- extrusion via cotransporters such as KCC2. Increasing Cl^- extrusion can increase the seizure threshold, help terminate seizures or prevent them altogether (Wang et al., 2018; Alfonsa et al., 2016; McMoneagle et al., 2024) while blocking KCC2 can allow seizures to start spontaneously (Sivakumaran et al., 2015). In agreement with this, in our simulations that accounted for Cl^- accumulation through $GABA_A$Rs and Cl^- extrusion through KCC2, we found that simulating sufficiently slow Cl^- extrusion in all neurons could cause a network to start bursting without further external provocation. Further, at fast Cl^- extrusion rates which resulted in low steady-state E_{GABA}, increasing $g_{GABAmax}$ reduced bursting, while at slow Cl^- extrusion rates, which resulted in high steady-state E_{GABA}, enhancing $g_{GABAmax}$ exacerbated bursting. Here, the steady-state E_{GABA} was not dependent on initial conditions. That is, the network's steady-state E_{GABA} ultimately reached the same value regardless of whether it started at physiological (−74 mV) or pathological (−51.6 mV) E_{GABA}. This result affirms the importance of Cl^- extrusion for affecting network excitability. Note that the E_{GABA} reported was an average of both PC and IN populations (at least one neuron from each), but each population would have a slightly different E_{GABA} because of differences in volume (see equation for dynamic E_{Cl}), as similarly reported experimentally (Burman et al., 2024).

By selectively altering Cl^- extrusion in each population of neurons (pyramidal vs interneuronal cells), we determined that Cl^- extrusion in pyramidal cells is the predominant factor for controlling SE-like activity while Cl^- extrusion in interneurons had only a minor influence. The failure of inhibitory connections from interneurons to pyramidal cells plays a key role in causing persistent bursting. The network was in SE-like activity if Cl^- extrusion in pyramidal cells was slow enough, regardless of Cl^- extrusion in interneurons. This suggests that focusing on reducing pyramidal cell Cl^- accumulation is a major avenue through which seizure activity can be arrested. This aligns with experimental findings where overexpression of KCC2, driven by a CaMKII promoter primarily targeting cortical pyramidal cells, reduced the seizure-promoting effect of excitatory interneuronal signalling (Magloire et al., 2019), although potential expression in interneurons cannot be fully excluded (Veres et al., 2023; Keaveney et al., 2020). This cell-type specific insight, attainable through the targeted manipulations possible in our computational model, highlights a potentially crucial target for future therapeutic interventions aimed at enhancing chloride extrusion specifically in principal neurons.

While we use a large, spiking neural network to simulate Cl^- dynamics, and apply this to model SE, previous computational models have explored the relevance of ion dynamics in SE using two-cell biophysical or mean-field approaches (Kramer et al., 2012; Krishnan and Bazhenov, 2011; Fröhlich et al., 2005). Our findings are in line with this work by reiterating the connection between raised intracellular Cl^- accumulation and E_{GABA} in maintaining extended seizures. Our model did not simulate dynamics in other ions including K^+, Na^+, H^+ and HCO_3^-, which are also known to both modulate and be modulated by seizure activity (Raimondo et al., 2015). These ions indirectly interact with Cl^- through at least two mechanisms: co-transporters like KCC2, which couple Cl^- transport to K^+, and receptors such as $GABA_A$Rs, which are permeable to both Cl^- and HCO_3^-. In addition to other ions, further work to extend the model could include modelling NKCC1 as well as dynamically changing the efficacy of channels and receptors as a function of phosphorylation and ATP availability throughout a simulation. Incorporating these additional biophysical details could enhance the accuracy of our simulations. In the context of a large network model such as this, however, it would come at a potentially prohibitive computational cost. Modelling the dynamics of other ions could also identify or confirm other, Cl^- independent mechanisms for aborting seizures. For example, enhancing intraneuronal H^+ (acidosis) is known to be anti-seizure via various mechanisms (Raimondo et al., 2015). Further, raised intraneuronal Na^+ has also been identified as contributing seizure termination (Krishnan and Bazhenov, 2011).

It is worth noting that our spiking neural network model was uniformly connected without explicitly modelling space or the propagation of activity through different brain regions. It did not capture potential spatial or inter-regional dynamics of activity-dependent shifts in E_{GABA}. Differences in neuronal E_{GABA} between brain regions could explain why many people with SE still respond to first-line treatment with benzodiazepines (Burman et al., 2022; Rahmati et al., 2021; Glykys et al., 2009; Colombi et al., 2024). In these patients it is possible that actively seizing networks with raised E_{GABA} are surrounded by less-affected areas with low E_{GABA} where benzodiazepines still enhance inhibition. The combined effect of a benzodiazepine likely depends on the extent to which various brain areas have been recruited into a seizure. Future work could extend our model by incorporating spatial considerations. Furthermore, our findings suggest a novel, mechanistically-informed strategy for optimising treatment, as depicted in our proposed decision framework (Fig. 5C). This framework offers translational potential by suggesting how observable clinical responses (e.g., EEG changes post-benzodiazepine) might predict the underlying state of Cl^- homeostasis and guide subsequent therapeutic choices, moving beyond purely empirical algorithms. Despite the model's spatial limitations, this consideration does not affect our major conclusion here, namely that should SE not abate following the initial delivery of a high dose of benzodiazepines, serious consideration should be paid to not repeatedly delivering further agents of this class. Second line treatment that also engages other non-Cl^- linked inhibitory systems should rather be considered. As one of multiple potential examples, this could include phenobarbital, which in addition to its effect on $GABA_A$Rs, is also an effective antagonist of AMPA and kainate glutamatergic receptors at higher concentrations (Macdonald and Barker, 1978; Nardou et al., 2011).

In summary, our simulations provide an experimentally supported method of investigating mechanisms in SE. Our findings therefore

predict that co-targeting of pyramidal cell extrusion with appropriate $GABA_AR$ conductance modulation represents a powerful potential strategy for terminating SE, an insight derived from our large-scale network model incorporating chloride dynamics. Although pharmacological enhancers of Cl^- extrusion via increasing the activity of KCC2 have been identified (Jarvis et al., 2023; McMoneagle et al., 2024), none have been cleared for clinical use. Regardless, this research reveals a promising avenue for future advances in the management of benzodiazepine resistant SE.

4. Materials and methods

4.1. In vivo paediatric EEG

Details of clinical recordings are fully explained in previous work (Fedele et al., 2025). In short, anonymised patient data was acquired retrospectively and was approved by the local ethics committee (Kantonale Ethikkommission Zürich, KEK-ZH PB-2020-02580). We extracted data from paediatric patients (under 18 years) with SE who underwent scalp EEG recordings between July 2008 and February 2020 at the University Children's Hospital Zurich. Clinical EEG recordings (21 electrodes, international 10–20 electrode layout, 256-Hz sampling) were reviewed and for the purposes of this study, illustrative examples of response to benzodiazepines were selected. To demonstrate the effect of benzodiazepine on the EEG signal, we isolated a 1000s epoch which included a 500 s window on either side of the administration. A virtual local field potential (vLFP) was extracted using Statistical Parametric Mapping (SPM12) to show the overall effect of benzodiazepine on the patients EEG. Spectrograms were generated using Morlet wavelets from the PyWavelets library (Lee et al., 2019).

4.2. In vitro brain slice gramicidin perforated patch clamp

Details of in vitro brain slice recordings are fully explained in previous work (Burman et al., 2019). Briefly, organotypic hippocampal slice cultures were prepared from mice. The use of animals was approved by the University of Cape Town Animal Ethics Committee. Recordings were performed 6–14 days post culture, equivalent to postnatal days 13 to 21 in mice and a paediatric age range in humans. Gramicidin perforated patch-clamp recordings were performed from CA1-CA3 hippocampal pyramidal cells using glass pipettes containing a high Cl^- internal solution containing (in mM): KCl (135), NaCl (8.9), HEPES (Chapman et al., 1977) and 80 mg/ml gramicidin. The standard artificial CSF was composed of (in mM): NaCl (120); KCl (Glauser et al., 2016); $MgCl_2$ (Boggs, 2004); $CaCl_2$ (Boggs, 2004); NaH_2PO_4 (1.2); $NaHCO_3$ (Ellender et al., 2014); D-glucose (Pereira de Vasconcelos et al., 1992) with pH adjusted to be between 7.35 and 7.40 using 0.1 mM NaOH. To elicit SE-like activity, slices were perfused with aCSF lacking Mg^{2+} (Anderson et al., 1986; Dreier and Heinemann, 1991). To measure E_{GABA} during SE-like activity, voltage ramps in voltage-clamp mode with and without GABA (100 μM) application directed to the cell soma were interleaved between measurements of spontaneous activity recorded in current-clamp mode (Burman et al., 2019; Ellender et al., 2014).

4.3. In silico model of status epilepticus

While the model is broadly informed by the clinical presentation of SE and experimental findings, key parameters were chosen to be quantitatively consistent with experimental observations. For instance, the simulated range of E_{GABA} values reflects experimentally measured shifts during SE-like activity (Fig. 1), and the magnitude of simulated $GABA_AR$ conductance modulations aligns with known pharmacological effects ("Modeling Pharmacological Modulation of $GABA_A$ Receptors" section below).

4.4. Spiking neural network population structure

We constructed a network of 1000 leaky integrate-and-fire point neurons with 20 % as the GABAergic interneuron (IN) population and 80 % as the glutamatergic pyramidal cell (PC) population (Brunel, 2000). Populations differed by their membrane capacitance, refractory period, and volume (see Table 1). The network had 2 % connectivity from the PC population, including recurrent connections, and 4 % connectivity from the IN population, also including recurrent connections, and 800 low frequency (2 Hz) Poisson inputs for sustained activity (Gerstner et al., 2014; Vogels et al., 2011).

4.5. Neuronal dynamics

Change in the neuronal membrane potential (V_m) was governed by

$$C_m\frac{dV_m}{dt} = -g_{leak}(V_m(t) - E_{leak}) - I_{syn}(t)$$

where g_{leak} (20 nS) and E_{leak} (−70 mV) are the conductance and reversal potential for the passive membrane channels respectively, C_m is the membrane capacitance (PC: 0.55 nF, IN: 0.45 nF) and I_{syn} is the synaptic current. Once threshold (−50 mV) was reached, a neuron would spike and reset (−65 mV) with a refractory period (PC: 2 ms, IN: 1 ms) during which a neuron could not spike again. Several mechanisms can enable a network to have bursts that occur over hundreds of milliseconds and seconds, including NMDA (Parga and Abbott, 2007; Wolf et al., 2005; Sanders et al., 2013) and short term synaptic plasticity (Melamed et al., 2008; Timofeev et al., 2000; Tsodyks and Markram, 1997), which were both incorporated.

4.6. Synaptic input currents and reversal potentials

Each neuron received synaptic input currents from AMPA, NMDA, and $GABA_A$ receptors, as well as low frequency (2 Hz) background AMPA input, modelled according to

$$I_{syn}(t) = I_{AMPA}(t) + I_{NMDA}(t) + I_{GABA}(t) + I_{AMPA_{2Hz}}(t)$$

$$I_{NMDA}(t) = \frac{g_{NMDA}(t)\ (V_m(t) - E_{NMDA})}{1 + \frac{[Mg^{2+}]e^{-0.062\ Vm}}{3.57}}$$

$$I_{AMPA}(t) = g_{AMPA}(t)\ (V_m(t) - E_{AMPA})$$

$$I_{GABA}(t) = g_{GABA}(t)\ (V_m(t) - E_{GABA}(t))$$

where E_{syn} is the reversal potential for that synapse, g_{syn} is the conductance for that synapse, and $[Mg^{2+}]$ is the magnesium block which was set to 0 mM within 5 s to mimic the in vitro experiments. The reversal potentials were $E_{NMDA} = 0$ mV, $E_{AMPA} = 0$ mV, and

$$E_{GABA}(t) = P_{Cl}E_{Cl}(t) + P_{HCO3}E_{HCO3}$$

The chord conductance formulation for the $GABA_AR$ reversal potential was used for its computational efficiency when modelling dynamic E_{Cl}. The chord conductance equation is a good first approximation for calculating the reversal potential of channels with multiple ions, simply following Kirchhoff's Current Law, albeit less accurate than the Goldman-Hodgkin-Katz equation. This formulation was chosen for its computational efficiency, which is advantageous for simulations within spiking neural networks, while still providing a reasonable approximation for E_{GABA}. The equation was derived as follows:

The total ionic current through the $GABA_A$ receptor is the sum of the currents carried by the permeant ions:

$$I_{GABA} = I_{Cl} + I_{HCO3}$$

The current for each ion (I_i) is approximated using its chord

Table 1
Symbols, Constants, and Parameters.

	Description	
Symbols		
AMPA	α-amino-3-hydroxy-5-methyl-4-isoxazolepropionic acid, which selectively activates the AMPA receptor	
AMPA receptor	Mediator of fast excitatory synaptic transmission when glutamate is bound	
Benzodiazepine	A class of drugs that positively modulate the conductance of $GABA_A$Rs	
Cl^-	Chloride ions	
$[Cl^-]_i$	Intracellular chloride concentration	
E_{syn}	Reversal potential, the value of which there is no net flow of current for that transmembrane channel or ion species	
g_{syn}	Conductance for a synapse	
GABA	γ-aminobutyric acid, the neurotransmitter released by interneurons	
$GABA_AR$	GABA type A receptor, which mediates fast inhibitory synaptic transmission when GABA is bound	
Glutamate	Primary neurotransmitter released by pyramidal cells in cortex and hippocampus	
HCO_3^-	Bicarbonate ions	
I_{Cl}	Chloride ion current through a channel	
I_{HCO3}	Bicarbonate ion current through a channel	
IN	Interneurons	
K^+	Potassium ion	
KCC2	Potassium chloride cotransporter type 2	
Mg^{2+}	Magnesium ion	
Na^+	Sodium ion	
NMDA	*N*-methyl-D-aspartate, which selectively activates the NMDA receptor	
NMDA receptor	Mediator of slow excitatory synaptic transmission when glutamate is bound	
PC	Pyramidal cell	
τ	Time constant, the time taken for the system to respond to change and reach either ≈ 63.2 % $\left(1 - {}^1/_e\right)$, for a step increase, or 36.8 % $\left({}^1/_e\right)$, for a step decrease, of its final steady-state value	
Constants		Value
F	Faraday's constant (approximate)	96,485 $s{\cdot}A{\cdot}mol^{-1}$
R	Ideal gas constant (approximate)	8.3145 $J{\cdot}K^{-1}{\cdot}mol^{-1}$
T	Absolute temperature (= 37 °C)	310.15 K
Parameters		Default Value
$AMPA_{2Hz}$	Background AMPA input	2 Hz
$[Cl^-]_o$	Extracellular chloride concentration	135 mM
C_m	Membrane capacitance	PC: 0.55 nF IN: 0.45 nF
Δt	Time step	100 μs
E_{leak}	Reversal potential for the leak channel	−70 mV
E_{AMPA}	Reversal potential for an AMPA receptor	0 mV
$E_{Cl}\infty$	Target reversal potential for chloride	−88 mV
E_{HCO3}	Reversal potential for bicarbonate ions	−18 mV
E_{NMDA}	Reversal potential for a NMDA receptor	0 mV
$g_{AMPAmax}$	Maximum conductance for an AMPA receptor	5 nS
$g_{AMPAmax,2Hz}$	Maximum conductance for background AMPA input	2 nS
$g_{GABAmax}$	Maximum conductance for a $GABA_A$ receptor	50 nS
g_{leak}	Conductance for the leak current	20 nS
$g_{NMDAmax}$	Maximum conductance for a NMDA receptor	5 nS
$[Mg^{2+}]$	Magnesium concentration for a NMDA receptor	0 mM
P_{Cl}	$GABA_AR$ permeability ratio for chloride ions	0.8
P_{HCO3}	$GABA_AR$ permeability ratio for bicarbonate ions	0.2
Refractory period	Time during which no spikes can be elicited	PC: 2 ms IN: 1 ms
τ_{AMPA}	Decay time constant for AMPA receptor (Ramaswamy et al., 2012)	2 ms
$\tau_{GABAdecay}$	Decay time constant for $GABA_A$ receptor	10 ms
τ_{KCC2}	Time constant of Cl^- extrusion	30 s
τ_{KCC2IN}	Decay time constant of Cl^- extrusion for IN	30 s
τ_{KCC2PC}	Decay time constant of Cl^- extrusion for PC	30 s
$\tau_{NMDAdecay}$	Decay time constant for NMDA receptor (Rhodes, 2006)	100 ms
$\tau_{NMDArise}$	Rise time constant for NMDA receptor (Rhodes, 2006)	2 ms
τ_d	Time constant for synaptic depression	10 s
τ_f	Time constant for synaptic facilitation	0.5 s
U_0	Step increase of release probability (u_s) per spike	0.01
V	Volume of neuronal compartment	PC: 220.9 μm^3 IN: 147.3 μm^3
V_{reset}	The voltage to which a neuron would reset after the refractory period	−65 mV
V_{thresh}	The voltage threshold for a neuron to spike	−50 mV
w_t	Relative time weight of NMDA's rise time	0.5 ms^{-1}
Variables		Initial Value
E_{Cl}	Reversal potential for chloride ions	−88 mV
E_{GABA}	Reversal potential for a $GABA_AR$	−74 mV
I_{GABA}	Total current through $GABA_AR$	0 mA
u_s	Synaptic release probability	0.01
ν	Firing rate of a neuron	2 Hz
V_m	Membrane potential	−60 ± 10 mV
w_{ij}	Connection strength to neuron i from neuron j	0.0002
x_s	Fraction of available neurotransmitters	0.02

conductance (g_i) and the driving force (V_m - E_i), where V_m is the membrane potential and E_i is the Nernst equilibrium potential for that ion so:

$$I_{Cl} = g_{Cl}(V_m - E_{Cl})$$

$$I_{HCO3} = g_{HCO3}(V_m - E_{HCO3})$$

By definition, the reversal potential (E_{GABA}) is the membrane potential (V_m) at which the net current through the channel is zero ($I_{GABA} = 0$). Substituting the ionic currents and setting $V_m = E_{GABA}$:

$$0 = g_{Cl}(E_{GABA} - E_{Cl}) + g_{HCO3}(E_{GABA} - E_{HCO3})$$

Rearranging the equation to solve for E_{GABA} yields:

$$E_{GABA} = \left(\frac{g_{Cl}}{g_{Cl} + g_{HCO3}}\right)E_{Cl} + \left(\frac{g_{HCO3}}{g_{Cl} + g_{HCO3}}\right)E_{HCO3}$$

P_{Cl} and P_{HCO3} represent the fractional conductances for Cl^- and HCO_3^-, respectively

$$P_{Cl} = \frac{g_{Cl}}{g_{Cl} + g_{HCO3}}$$

$$P_{HCO3} = \frac{g_{HCO3}}{g_{Cl} + g_{HCO3}}$$

and represent the relative contribution of each ion's conductance to the total channel conductance ($g_{Cl} + g_{HCO3}$) and sum to unity. We used channel permeability ratios P_{Cl}: $P_{HCO3} = 0.8$: 0.2 (Bormann et al., 1987). Where $E_{Cl} = -88$ mV (for static Cl^- simulations) and $E_{HCO3} = -18$ mV, E_{GABA} was −74 mV. Previous work of ours has focused on accurately modelling dynamic E_{GABA} and E_{Cl} in dendrites using the Goldman-Hodgkin-Katz and Nernst equations, respectively (Currin and Raimondo, 2022).

4.7. Dynamic GABA and chloride reversal potentials

For dynamic Cl^- simulations (Figs. 3, 4, and 5), E_{Cl} was modelled according to

$$\frac{d}{dt}E_{Cl} = \underbrace{\frac{I_{Cl}(t)}{\beta \exp(\beta\, E_{Cl}(t)\,) F\, V\, [Cl^-]_o}}_{\text{influx}} - \underbrace{\frac{E_{Cl}(t) - E_{Cl}^{\infty}}{\tau_{KCC2}}}_{\text{extrusion}}$$

with

$$I_{Cl}(t) = g_{GABA}(t)\, P_{Cl}\, (V_m(t) - E_{Cl}(t)\,)$$

$$\beta = \frac{F}{R\, T}$$

where R is the ideal gas constant, T is the temperature in Kelvin, F is Faraday's constant, V is the neuronal volume (PC: 220.9 μm^3, IN: 147.3 μm^3), $[Cl^-]_o$ is the external Cl^- concentration, I_{Cl} is the Cl^- current through a $GABA_AR$, $E_{Cl}\infty$ is the target reversal potential for Cl^- (−88 mV) and τ_{KCC2} is the time constant for KCC2. See Supplementary Information for derivation details of influx, and extrusion was modelled akin to (Jedlicka et al., 2011b).

4.8. Synaptic conductances with short-term plasticity

The change in synaptic conductance was modelled as a single- or double-exponential curve. AMPA and $GABA_A$ synapses were modelled as

$$\frac{d}{dt}g_{syn} = -\frac{g_{syn}(t)}{\tau_{syn}}$$

where τ_{syn} is the decay time constant ($\tau_{AMPA} = 2$ ms, $\tau_{GABA} = 10$ ms). NMDA conductance was modelled as

$$\frac{d}{dt}g_{NMDA} = -\frac{g_{NMDA}(t)}{\tau_{decay}} + w_t\, r(t)\, (1 - g_{NMDA}(t)\,)$$

$$\frac{d}{dt}r = -\frac{r(t)}{\tau_{rise}}$$

where τ_{decay} is the decay time constant for NMDA (100 ms), τ_{rise} is the rise time constant for NMDA (2 ms), r is the exponential rise component of the conductance, and w_t is its relative time weight (0.5 ms^{-1}). Incoming synaptic conductances were calculated according to

$$g_{syn}(t) = \int_{t-\Delta t}^{t} g_{syn_{max}}\, w_{ij}(t)\, \delta(t - t_{spk})\, dt$$

where g_{synmax} is the max synaptic conductance ($g_{AMPAmax,2Hz} = 2$ nS, $g_{AMPAmax} = 5$ nS, $g_{NMDAmax} = 5$ nS, $g_{GABAmax} = 50$ nS), w_{ij} is the connection strength ('weight') for neuron i from neuron j (see details below), δ is the Dirac delta function, t_{spk} is the spike time of the presynaptic neuron, and Δt is the integration time window (100 μs).

4.9. The connection strength of a synapse (w_{ij}) was modelled using short-term plasticity (STP) (Melamed et al., 2008) and defined according to

$$w_{ij}(t) = u_s(t)\, x_s(t)$$

where u_s is facilitation – the release probability of neurotransmitters – and x_s is depression – the amount of neurotransmitter available. These variables obeyed the following dynamics:

$$\frac{du_s}{dt} = -\frac{u_s(t)}{\tau_f} + U_0\, (1 - u_s(t)\,)\, \upsilon(t) \frac{dx_s}{dt} = \frac{(1 - x_s(t)\,)}{\tau_d} - x_s(t)\, u_s(t)\, \upsilon(t.)$$

where U_0 is the step increase in u_s per spike (0.01), τ_f is the time constant for facilitation (0.5 s), τ_d is the time constant for depression (10 s), and υ is the firing rate of presynaptic neuron j for a given time window ($\Delta t = 100$ μs) and calculated as

$$\nu(t) = \frac{1}{\Delta t}\int_{t-\Delta t}^{t} \delta(t - t_{spk})\, dt.$$

4.10. Modelling pharmacological modulation of $GABA_A$ receptors

To simulate the effects of pharmacological agents targeting $GABA_A$ receptors, the maximal $GABA_AR$ conductance ($g_{GABAmax}$) was modulated to a range of values including 0, 0.25 0.5, 1, 2, 4 and 8 times the baseline (50 nS). For simulating the effect of benzodiazepines or barbiturates, which act as positive allosteric modulators, $g_{GABAmax}$ was typically increased up to 2 or 4-fold. This factor was chosen because experimental studies show that potentiation saturates, typically resulting in a 2- to 3-fold increase in GABA-evoked currents or conductance, making a 2 or 4-fold increase a reasonable upper bound for the maximal effect (Burman et al., 2019; Rogers et al., 1994; Macdonald and Barker, 1978; Nardou et al., 2011; Birnir et al., 2000). To simulate the effect of high-dose phenobarbital, in addition to a 4-fold increase in $g_{GABAmax}$, $g_{AMPAmax}$ was reduced to 87.5 % of baseline (Nardou et al., 2011). To simulate the effect of picrotoxin, a non-competitive $GABA_AR$ antagonist, $g_{GABAmax}$ was decreased 2 or 4-fold (representing 50 % or 75 % inhibition). This reflects the concentration-dependent and often partial block observed experimentally, where significant inhibition (e.g., 60–90 %) occurs at commonly used micromolar concentrations (e.g., 10–30 μM) (Twyman et al., 1989), and aligns with kinetic studies suggesting picrotoxin decreases the channel-opening equilibrium constant by approximately 4-fold (Ramakrishnan and Hess, 2005).

4.11. Simulation details

Simulations were carried out using the Brian2 Python package (Stimberg et al., 2019), with C++ standalone code generation. Brian2's default time step of 100 μs and the default numerical integration method of forward Euler were used. E_{GABA} was averaged over simulations ($n \geq 5$) from at least one PC and IN per simulation. Network bursting activity was quantified based on the population firing rate, calculated using a sliding time window. A burst was detected if the population firing rate exceeded 20 Hz and was simultaneously more than two standard deviations above the baseline firing rate (calculated during a non-bursting period) for a minimum duration of 20 ms. For each detected burst, the *duration* was measured as the continuous period of time during which the population firing rate remained above the 20 Hz threshold. The *amplitude* of the burst was calculated as the difference between the peak population firing rate achieved during the burst and the population firing rate recorded at the onset time of the burst (i.e., the time point when the detection criteria were first met). Burst frequency (number of bursts per unit time, e.g., per minute) was calculated over specific simulation epochs as indicated in the relevant figure legends.

All model source code (available online at https://github.com/ChrisCurrin/goldilocks-GABA) was written in Python with data processing performed using NumPy (Harris et al., 2020), SciPy (Virtanen et al., 2020), and Pandas (McKinney, 2010). Results were plotted using the Matplotlib and Seaborn libraries (Hunter, 2007; Waskom, 2020).

CRediT authorship contribution statement

Christopher B. Currin: Writing – review & editing, Writing – original draft, Visualization, Software, Methodology, Investigation, Funding acquisition, Formal analysis, Conceptualization. **Richard J. Burman:** Writing – review & editing, Writing – original draft, Visualization, Investigation, Formal analysis, Data curation. **Tommaso Fedele:** Writing – review & editing, Investigation. **Georgia Ramantani:** Investigation. **Richard E. Rosch:** Writing – review & editing, Investigation. **Henning Sprekeler:** Writing – review & editing, Supervision, Methodology. **Joseph V. Raimondo:** Writing – review & editing, Supervision, Project administration, Conceptualization.

Declaration of competing interest

None of the authors has any conflict of interest to disclose

Acknowledgements

The research leading to these results has received support from the National Research Foundation of South Africa, the Deutscher Akademischer Austauschdienst, NOMIS Foundation, NVIDIA Academic Program, the University of Cape Town, the Anna Mueller Grocholski Foundation, the Swiss National Science Foundation (SNSF: 208184), the Gabriel Foundation, a Wellcome Trust Seed Award (214042/Z/18/Z), the South African Medical Research Council and the FLAIR Fellowship Programme (FLR\R1\190829): a partnership between the African Academy of Sciences and the Royal Society funded by the UK Government's Global Challenges Research Fund and a Wellcome Trust International Intermediate Fellowship (222968/Z/21/Z).

Appendix A. Supplementary data

Supplementary data to this article can be found online at https://doi.org/10.1016/j.nbd.2025.106966.

Data availability

Data and code are available via links in the manuscript or upon request

References

Alfonsa, H., Lakey, J.H., Lightowlers, R.N., Trevelyan, A.J., 2016. Cl-out is a novel cooperative optogenetic tool for extruding chloride from neurons. Nat. Commun. 7. https://doi.org/10.1038/ncomms13495.

Anderson, W.W., Lewis, D.V., Swartzwelder, H.S., Wilson, W.A., 1986. Magnesium-free medium activates seizure-like events in the rat hippocampal slice. Brain Res. 398, 215–219.

Appleton, R., Choonara, I., Martland, T., Phillips, B., Scott, R., Whitehouse, W., 2000. The treatment of convulsive status epilepticus in children. Arch. Dis. Child. 83, 415–419.

Ben-Ari, Y., 2002. Excitatory actions of GABA during development: the nature of the nurture. Nat. Rev. Neurosci. 3, 728–739.

Birnir, B., Eghbali, M., Everitt, A.B., Gage, P.W., 2000. Bicuculline, pentobarbital and diazepam modulate spontaneous GABAA channels in rat hippocampal neurons. Br. J. Pharmacol. 131, 695–704.

Boggs, J.G., 2004. Mortality associated with status epilepticus. Epilepsy Currents 4, 25–27.

Bormann, J., Hamill, O.P., Sakmann, B., 1987. Mechanism of anion permeation through channels gated by glycine and gamma-aminobutyric acid in mouse cultured spinal neurones. J. Physiol. 385, 243–286.

Browne, T.R., Penry, J.K., 1973. Benzodiazepines in the treatment of epilepsy a review. Epilepsia 14, 277–310.

Brunel, N., 2000. Phase diagrams of sparsely connected networks of excitatory and inhibitory spiking neurons. Neurocomputing 32–33, 307–312.

Burman, R.J., Selfe, J.S., Lee, J.H., van den Berg, M., Calin, A., Codadu, N.K., Wright, R., Newey, S.E., Parrish, R.R., Katz, A.A., Wilmshurst, J.M., Akerman, C.J., Trevelyan, A.J., Raimondo, J.V., 2019. Excitatory GABAergic signalling is associated with benzodiazepine resistance in status epilepticus. Brain 142, 3482–3501.

Burman, R.J., Raimondo, J.V., Jefferys, J.G.R., Sen, A., Akerman, C.J., 2020. The transition to status epilepticus: how the brain meets the demands of perpetual seizure activity. Seizure 75, 137–144.

Burman, R.J., Rosch, R.E., Wilmshurst, J.M., Sen, A., Ramantani, G., Akerman, C.J., Raimondo, J.V., 2022. Why won't it stop? The dynamics of benzodiazepine resistance in status epilepticus. Nat. Rev. Neurol. 18, 428–441.

Burman, R.J., Diviney, T., Călin, A., Gothard, G., Jouhanneau, J.-S.M., Poulet, J.F.A., Sen, A., Akerman, C.J., 2024. Optogenetic determination of dynamic and cell-type-specific inhibitory reversal potentials. J. Neurosci. https://doi.org/10.1523/JNEUROSCI.1392-23.2024.

Chapman, A.G., Meldrum, B.S., Siesiö, B.K., 1977. Cerebral metabolic changes during prolonged epileptic seizures in rats. J. Neurochem. 28, 1025–1035.

Cheung, D.L., Cooke, M.J., Goulton, C.S., Chaichim, C., Cheung, L.F., Khoshaba, A., Nabekura, J., Moorhouse, A.J., 2022. Global transgenic upregulation of KCC2 confers enhanced diazepam efficacy in treating sustained seizures. Epilepsia 63, e15–e22.

Chin, R.F., Neville, B.G., Peckham, C., Wade, A., Bedford, H., Scott, R.C., 2008. Treatment of community-onset, childhood convulsive status epilepticus: a prospective, population-based study. Lancet Neurol. 7, 696–703.

Codadu, N.K., Graham, R.T., Burman, R.J., Jackson-Taylor, R.T., Raimondo, J.V., Trevelyan, A.J., Parrish, R.R., 2019. Divergent paths to seizure-like events. Phys. Rep. 7, 1–15.

Colombi, I., Rastogi, M., Parrini, M., Alberti, M., Potenzieri, A., Chellali, M.M., Rosati, S., Chiappalone, M., Nanni, M., Contestabile, A., Cancedda, L., 2024. Heterogeneous subpopulations of GABAAR-responding neurons coexist across neuronal network scales and developmental stages in health and disease. iScience 27, 109438.

Currin, C.B., Raimondo, J.V., 2022. Computational models reveal how chloride dynamics determine the optimal distribution of inhibitory synapses to minimise dendritic excitability. PLoS Comput. Biol. 18, e1010534.

Currin, C.B., Trevelyan, A.J., Akerman, C.J., Raimondo, J.V., Berry, H. (Eds.), 2020. PLoS Comput. Biol. 16, e1007932.

Currin, C.B., Raimondo, J.V., Rubin, J., 2022. Computational models reveal how chloride dynamics determine the optimal distribution of inhibitory synapses to minimise dendritic excitability. PLoS Comput. Biol. 18, e1010534.

Deeb, T.Z., Maguire, J., Moss, S.J., 2012. Possible alterations in GABAA receptor signaling that underlie benzodiazepine-resistant seizures. Epilepsia 53, 79–88.

Deshpande, L.S., Blair, R.E., Nagarkatti, N., Sombati, S., Martin, B.R., DeLorenzo, R.J., 2007. Development of pharmacoresistance to benzodiazepines but not cannabinoids in the hippocampal neuronal culture model of status epilepticus. Exp. Neurol. 204, 705–713.

Doyon, N., Prescott, S.A., Castonguay, A., Godin, A.G., Kröger, H., De Koninck, Y., 2011. Efficacy of synaptic inhibition depends on multiple, dynamically interacting mechanisms implicated in chloride homeostasis. PLoS Comput. Biol. 7, 1–22.

Dreier, J.P., Heinemann, U., 1991. Regional and time dependent variations of low Mg2+ induced epileptiform activity in rat temporal cortex slices. Exp. Brain Res. 87, 581–596.

El Hamdi, G., Pereira de Vasconcelos, A., Vert, P., Nehlig, A., 1992. An experimental model of generalized seizures for the measurement of local cerebral glucose utilization in the immature rat. I. Behavioral characterization and determination of lumped constant. Dev. Brain Res. 69, 233–242.

Ellender, T.J., Raimondo, J.V., Irkle, A., Lamsa, K.P., Akerman, C.J., 2014. Excitatory effects of Parvalbumin-expressing interneurons maintain hippocampal epileptiform activity via synchronous Afterdischarges. J. Neurosci. 34, 15208–15222.

Farrant, M., Kaila, K., 2007. The cellular, molecular and ionic basis of GABAA receptor signalling. Prog. Brain Res. 160, 59–87.

Fröhlich, F., Bazhenov, M., Timofeev, I., Sejnowski, T.J., 2005. Maintenance and termination of neocortical oscillations by dynamic modulation of intrinsic and synaptic excitability. Thalamus Relat. Syst. 3, 147–156.

Gaínza-Lein, M., Sánchez Fernández, I., Jackson, M., Abend, N.S., Arya, R., Brenton, J.N., Carpenter, J.L., Chapman, K.E., Gaillard, W.D., Glauser, T.A., Goldstein, J.L., Goodkin, H.P., Kapur, K., Mikati, M.A., Pearlso, K., Tasker, R.C., Tchapyjnikov, D., Topjian, A.A., Wainwright, M.S., Wilfong, A., Williams, K., Loddenkemper, T., Pediatric Status Epilepticus Research Group, 2018. Association of time to treatment with short-term outcomes for pediatric patients with refractory convulsive status epilepticus. JAMA Neurol. 75, 410–418.

Gerstner, W., Kistler, W.M., Naud, R., Paninski, L., 2014. In: Gerstner, W., Kistler, W.M., Naud, R., Paninski, L. (Eds.), Neuronal Dynamics. Cambridge University Press, Cambridge. https://neuronaldynamics.epfl.ch/index.html.

Glauser, T., Shinnar, S., Gloss, D., Alldredge, B., Arya, R., Bainbridge, J., Bare, M., Bleck, T., Edwin Dodson, W., Garrity, L., Jagoda, A., Lowenstein, D., Pellock, J., Riviello, J., Sloan, E., Treiman, D.M., 2016. Evidence-based guideline: treatment of convulsive status epilepticus in children and adults: report of the guideline committee of the American epilepsy society. Epilepsy Currents 16, 48–61.

Glykys, J., Dzhala, V.I., Kuchibhotla, K.V., Feng, G., Kuner, T., Augustine, G., Bacskai, B. J., Staley, K.J., 2009. Differences in cortical versus subcortical GABAergic signaling: a candidate mechanism of Electroclinical uncoupling of neonatal seizures. Neuron 63, 657–672.

Goodkin, H.P., Yeh, J.-L., Kapur, J., 2005. Status epilepticus increases the intracellular accumulation of GABAA receptors. J. Neurosci. 25, 5511–5520.

Goodkin, H.P., Joshi, S., Mtchedlishvili, Z., Brar, J., Kapur, J., 2008. Subunit-specific trafficking of GABAA receptors during status epilepticus. J. Neurosci. 28, 2527–2538.

Harris, C.R., Millman, K.J., van der Walt, S.J., Gommers, R., Virtanen, P., Cournapeau, D., Wieser, E., Taylor, J., Berg, S., Smith, N.J., Kern, R., Picus, M., Hoyer, S., van Kerkwijk, M.H., Brett, M., Haldane, A., del Río, J.F., Wiebe, M., Peterson, P., Gérard-Marchant, P., Sheppard, K., Reddy, T., Weckesser, W., Abbasi, H., Gohlke, C., Oliphant, T.E., 2020. Array programming with NumPy. Nature 585, 357–362.

Huberfeld, G., Wittner, L., Clemenceau, S., Baulac, M., Kaila, K., Miles, R., Rivera, C., 2007. Perturbed chloride homeostasis and GABAergic signaling in human temporal lobe epilepsy. J. Neurosci. 27, 9866–9873.

Hunter, J.D., 2007. Matplotlib: a 2D graphics environment. Comput. Sci. Eng. 9, 90–95.

Jarvis, R., Josephine Ng, S.F., Nathanson, A.J., Cardarelli, R.A., Abiraman, K., Wade, F., Evans-Strong, A., Fernandez-Campa, M.P., Deeb, T.Z., Smalley, J.L., Jamier, T., Gurrell, I.K., McWilliams, L., Kawatkar, A., Conway, L.C., Wang, Q., Burli, R.W., Brandon, N.J., Chessell, I.P., Goldman, A.J., Maguire, J.L., Moss, S.J., 2023. Direct activation of KCC2 arrests benzodiazepine refractory status epilepticus and limits the subsequent neuronal injury in mice. Cell Re. Med. 4, 100957.

Jedlicka, P., Deller, T., Gutkin, B., 2011a. Activity dependent intracellular chloride accumulation and diffusion controls GABAA receptor mediated synaptic transmission. Hippocampus 898, 885–898.

Jedlicka, P., Deller, T., Gutkin, B.S., Backus, K.H., 2011b. Activity-dependent intracellular chloride accumulation and diffusion controls GABA(a) receptor-mediated synaptic transmission. Hippocampus 21, 885–898.

Kaila, K., Price, T.J., Payne, J.A., Puskarjov, M., Voipio, J., 2014. Cation-chloride cotransporters in neuronal development, plasticity and disease. Nat. Rev. Neurosci. 15, 637–654.
Kapur, J., Coulter, D.A., 1995. Experimental status epilepticus alters gamma-aminobutyric acid type A receptor function in CA1 pyramidal neurons. Ann. Neurol. 38, 893–900.
Keaveney, M.K., Rahsepar, B., Tseng, H., Fernandez, F.R., Mount, R.A., Ta, T., White, J. A., Berg, J., Han, X., 2020. CaMKIIα-positive interneurons identified via a microRNA-based viral gene targeting strategy. J. Neurosci. 40, 9576–9588.
Kramer, M.A., Truccolo, W., Eden, U.T., Lepage, K.Q., Hochberg, L.R., Eskandar, E.N., Madsen, Joseph R., Lee, J.W., Maheshwari, A., Halgren, E., Chu, C.J., Cash, S.S., 2012. Human seizures self-terminate across spatial scales via a critical transition. In: Proceedings of the National Academy of Sciences, 109, pp. 21116–21121.
Krishnan, G.P., Bazhenov, M., 2011. Ionic dynamics mediate spontaneous termination of seizures and postictal depression state. J. Neurosci. 31, 8870–8882.
Lee, H.H.C., Deeb, T.Z., Walker, J.A., Davies, P.A., Moss, S.J., 2011. NMDA receptor activity downregulates KCC2 resulting in depolarizing GABAA receptor–mediated currents. Nat. Neurosci. 14, 736–743.
Lee, G.R., Gommers, R., Waselewski, F., Wohlfahrt, K., O'Leary, A., 2019. PyWavelets: a Python package for wavelet analysis. J. Open Source Software 4, 1237.
Macdonald, R.L., Barker, J.L., 1978. Different actions of anticonvulsant and anesthetic barbiturates revealed by use of cultured mammalian neurons. Science 200, 775–777.
Magloire, V., Cornford, J., Lieb, A., Kullmann, D.M., Pavlov, I., 2019. KCC2 overexpression prevents the paradoxical seizure-promoting action of somatic inhibition. Nat. Commun. 10, 1225.
Mayer, S.A., Claassen, J., Lokin, J., Mendelsohn, F., Dennis, L.J., Fitzsimmons, B.F., 2002. Refractory status epilepticus: frequency, risk factors, and impact on outcome. Arch. Neurol. 59, 205–210.
McKinney, W., 2010. Data Structures for Statistical Computing in Python. In: Proceedings of the 9th Python in Science Conference 1697900, pp. 51–56.
McMoneagle, E., Zhou, J., Zhang, S., Huang, W., Josiah, S.S., Ding, K., Wang, Y., Zhang, J., 2024. Neuronal K+-cl- cotransporter KCC2 as a promising drug target for epilepsy treatment. Acta Pharmacol. Sin. 45, 1–22.
Melamed, O., Barak, O., Silberberg, G., Markram, H., Tsodyks, M., 2008. Slow oscillations in neural networks with facilitating synapses. J. Comput. Neurosci. 25, 308–316.
Miles, R., Wong, R.K.S., Traub, R.D., 1984. Synchronized afterdischarges in the hippocampus: contribution of local synaptic interactions. Neuroscience 12, 1179–1189.
Nardou, R., Yamamoto, S., Bhar, A., Burnashev, N., Ben-Ari, Y., Khalilov, I., 2011. Phenobarbital but not diazepam reduces AMPA/kainate receptor mediated currents and exerts opposite actions on initial seizures in the neonatal rat Hippocampus. Front. Cell. Neurosci. 5, 1–16.
Nehlig, A., Pereira de Vasconcelos, A., 1996. The model of pentylenetetrazol-induced status epilepticus in the immature rat: short- and long-term effects. Epilepsy Res. 26, 93–103.
Parga, N., Abbott, L.F., 2007. Network model of spontaneous activity exhibiting synchronous transitions between up and down states. Front. Neurosci. 1, 57–66.
Pereira de Vasconcelos, A., el Hamdi, G., Vert, P., Nehlig, A., 1992. An experimental model of generalized seizures for the measurement of local cerebral glucose utilization in the immature rat. II. Mapping of brain metabolism using the quantitative [14C]2-deoxyglucose technique. Brain Res. Dev. Brain Res. vol. 69, 243–259.
Pitkanen, A., Schwartzkroin, P., Moshe, S., 2006. Models of Seizures and Epilepsy. https://books.google.co.za/books?hl=en&lr=&id=qUXUDQAAQBAJ&oi=fnd&pg=PP1&dq=Models+of+Seizures+and+Epilepsy&ots=t56bP35Mwq&sig=_ooevDMUzoMOAdmuztwLNEEbp3k#v=onepage&q=ModelsofSeizuresandEpilepsy&f=false.
Rahmati, N., Normoyle, K.P., Glykys, J., Dzhala, V.I., Lillis, K.P., Kahle, K.T., Raiyyani, R., Jacob, T., Staley, K.J., 2021. Unique actions of GABA arising from cytoplasmic chloride microdomains. J. Neurosci. 41, 4957–4975.
Raimondo, J.V., Markram, H., Akerman, C.J., 2012. Short-term ionic plasticity at GABAergic synapses. Front. Synaptic Neurosci. 4, 1–9.
Raimondo, J.V., Burman, R.J., Katz, A.A., Akerman, C.J., 2015. Ion dynamics during seizures. Front. Cell. Neurosci. 9, 1–14.
Raimondo, J.V., Richards, B.A., Woodin, M.A., 2017. Neuronal chloride and excitability — the big impact of small changes. Curr. Opin. Neurobiol. 43, 35–42.
Ramakrishnan, L., Hess, G.P., 2005. Picrotoxin inhibition mechanism of a γ-aminobutyric AcidA receptor investigated by a laser-pulse photolysis technique. Biochemistry 44, 8523–8532.
Ramaswamy, S., Hill, S.L., King, J.G., Schürmann, F., Wang, Y., Markram, H., 2012. Intrinsic morphological diversity of thick-tufted layer 5 pyramidal neurons ensures robust and invariant properties of *in silico* synaptic connections. J. Physiol. 590, 737–752.
Rhodes, P., 2006. The properties and implications of NMDA spikes in neocortical pyramidal cells. J. Neurosci. 26, 6704–6715.
Rivera, C., Voipio, J., Thomas-Crusells, J., Li, H., Emri, Z., Sipilä, S., Payne, J.A., Minichiello, L., Saarma, M., Kaila, K., 2004. Mechanism of activity-dependent downregulation of the neuron-specific K-cl cotransporter KCC2. J. Neurosci. 24, 4683–4691.
Rogers, C.J., Twyman, R.E., Macdonald, R.L., 1994. Benzodiazepine and beta-carboline regulation of single GABAA receptor channels of mouse spinal neurones in culture. J. Physiol. 475, 69–82.
Sanders, H., Berends, M., Major, G., Goldman, M.S., Lisman, J.E., 2013. NMDA and GABAB (KIR) conductances: the "perfect couple" for bistability. J. Neurosci. 33, 424–429.
Sivakumaran, S., Maguire, J., 2016. Bumetanide reduces seizure progression and the development of pharmacoresistant status epilepticus. Epilepsia 57, 222–232.
Sivakumaran, S., Cardarelli, R.A., Maguire, J., Kelley, M.R., Silayeva, L., Morrow, D.H., Mukherjee, J., Moore, Y.E., Mather, R.J., Duggan, M.E., Brandon, N.J., Dunlop, J., Zicha, S., Moss, S.J., Deeb, T.Z., 2015. Selective inhibition of KCC2 leads to hyperexcitability and epileptiform discharges in hippocampal slices and in vivo. J. Neurosci. 35, 8291–8296.
Staley, K., 1992. Enhancement of the excitatory actions of GABA by barbiturates and benzodiazepines. Neurosci. Lett. 146, 105–107.
Stimberg, M., Brette, R., Goodman, D.F.M., 2019. Brian 2, an intuitive and efficient neural simulator. eLife 8. https://doi.org/10.7554/eLife.47314.
Sulis Sato, S., Artoni, P., Landi, S., Cozzolino, O., Parra, R., Pracucci, E., Trovato, F., Szczurkowska, J., Luin, S., Arosio, D., Beltram, F., Cancedda, L., Kaila, K., Ratto, G. M., 2017. Simultaneous two-photon imaging of intracellular chloride concentration and pH in mouse pyramidal neurons in vivo. Proc. Natl. Acad. Sci. 114, E8770–E8779, 201702861.
Timofeev, I., Grenier, F., Bazhenov, M., Sejnowski, T.J., Steriade, M., 2000. Origin of slow cortical oscillations in deafferented cortical slabs. Cereb. Cortex 10, 1185–1199.
Trevelyan, A.J., Schevon, C.A., 2013. How inhibition influences seizure propagation. Neuropharmacology 69, 45–54.
Trinka, E., Cock, H., Hesdorffer, D., Rossetti, A.O., Scheffer, I.E., Shinnar, S., Shorvon, S., Lowenstein, D.H., 2015. A definition and classification of status epilepticus - report of the ILAE task force on classification of status epilepticus. Epilepsia 56, 1515–1523.
Tsodyks, M., Markram, H., 1997. The neural code between neocortical pyramidal neurons depends on neurotransmitter release probability. Proc. Natl. Acad. Sci. USA 94, 719–723.
Twyman, R.E., Rogers, C.J., Macdonald, R.L., 1989. Pentobarbital and picrotoxin have reciprocal actions on single GABAA receptor channels. Neurosci. Lett. 96, 89–95.
Veres, J.M., Andrasi, T., Nagy-Pal, P., Hajos, N., 2023. CaMKIIα promoter-controlled circuit manipulations target both pyramidal cells and inhibitory interneurons in cortical networks. eNeuro 10. https://doi.org/10.1523/ENEURO.0070-23.2023.
Viitanen, T., Ruusuvuori, E., Kaila, K., Voipio, J., 2010. The K+-cl− cotransporter KCC2 promotes GABAergic excitation in the mature rat hippocampus. J. Physiol. 588, 1527–1540.
Fedele, T., Burman, R.J., Steinberg, A., Selmin, G., Ramantani, G., Rosch, R.E., 2025. Synaptic inhibitory dynamics drive benzodiazepine response in pediatric status epilepticus. Epilepsia 00, 1–15.
P. Virtanen, R. Gommers, T. E. Oliphant, M. Haberland, T. Reddy, D. Cournapeau, E. Burovski, P. Peterson, W. Weckesser, J. Bright, S. J. van der Walt, M. Brett, J. Wilson, K. J. Millman, N. Mayorov, A. R. J. Nelson, E. Jones, R. Kern, E. Larson, C. J. Carey, İ. Polat, Y. Feng, E. W. Moore, J. VanderPlas, D. Laxalde, J. Perktold, R. Cimrman, I. Henriksen, E. A. Quintero, C. R. Harris, A. M. Archibald, A. H. Ribeiro, F. Pedregosa, P. van Mulbregt, A. Vijaykumar, A. P. Bardelli, A. Rothberg, A. Hilboll, A. Kloeckner, A. Scopatz, A. Lee, A. Rokem, C. N. Woods, C. Fulton, C. Masson, C. Häggström, C. Fitzgerald, D. A. Nicholson, D. R. Hagen, D. V. Pasechnik, E. Olivetti, E. Martin, E. Wieser, F. Silva, F. Lenders, F. Wilhelm, G. Young, G. A. Price, G. L. Ingold, G. E. Allen, G. R. Lee, H. Audren, I. Probst, J. P. Dietrich, J. Silterra, J. T. Webber, J. Slavič, J. Nothman, J. Buchner, J. Kulick, J. L. Schönberger, J. V. de Miranda Cardoso, J. Reimer, J. Harrington, J. L. C. Rodríguez, J. Nunez-Iglesias, J. Kuczynski, K. Tritz, M. Thoma, M. Newville, M. Kümmerer, M. Bolingbroke, M. Tartre, M. Pak, N. J. Smith, N. Nowaczyk, N. Shebanov, O. Pavlyk, P. A. Brodtkorb, P. Lee, R. T. McGibbon, R. Feldbauer, S. Lewis, S. Tygier, S. Sievert, S. Vigna, S. Peterson, S. More, T. Pudlik, T. Oshima, T. J. Pingel, T. P. Robitaille, T. Spura, T. R. Jones, T. Cera, T. Leslie, T. Zito, T. Krauss, U. Upadhyay, Y. O. Halchenko, Y. Vázquez-Baeza, SciPy 1.0: fundamental algorithms for scientific computing in Python. Nat. Methods 17, 261–272 (2020).
Vogels, T.P., Sprekeler, H., Zenke, F., Clopath, C., Gerstner, W., 2011. Inhibitory plasticity balances excitation and inhibition in sensory pathways and memory networks. Science 334, 1569–1573.
Wang, Y., Wang, Y., Chen, Z., 2018. Double-edged GABAergic synaptic transmission in seizures: the importance of chloride plasticity. Brain Res. 1701, 126–136.
Waskom, M., 2020. The seaborn development team, mwaskom/seaborn. https://doi.org/10.5281/zenodo.592845.
Wenzel, M., Hamm, J.P., Peterka, D.S., Correspondence, R.Y., Yuste, R., 2017. Reliable and elastic propagation of cortical seizures in vivo. Cell Rep. 19, 2681–2693.
Wolf, J.A., Moyer, J.T., Lazarewicz, M.T., Contreras, D., Benoit-Marand, M., O'Donnell, P., Finkel, L.H., 2005. NMDA/AMPA ratio impacts state transitions and entrainment to oscillations in a computational model of the nucleus accumbens medium spiny projection neuron. J. Neurosci. 25, 9080–9095.